A stabilized displacement-volumetric strain formulation for nearly incompressible and anisotropic materials

R. Rossi[a,b,*], R. Zorrilla[a,b], R. Codina[a,b]

[a] *Universitat Politècnica de Catalunya (UPC), Departament d'Enginyeria Civil i Ambiental, Spain*
[b] *International Center for Numerical Methods in Engineering (CIMNE), Spain*

Abstract

The simulation of structural problems involving the deformations of volumetric bodies is of paramount importance is many areas of engineering. Although the use of tetrahedral elements is extremely appealing, tetrahedral discretizations are generally known as very stiff and are hence often avoided in typical simulation workflows. The development of mixed displacement-pressure approaches has allowed to effectively overcome this problem leading to a class of locking-free elements which can effectively compete with hexahedral discretizations while retaining obvious advantages in the mesh generation step. Despite such advantages the adoption of the technology within commercial codes is not yet pervasive. This can be attributed to two different reasons: the difficulty in making use of standard constitutive libraries and the implied continuity of the pressure, which makes questionable the application of the method in the context of multi-material problems. Current paper proposes the adoption of the volumetric strain instead of the pressure as nodal value. Such choice leads naturally to the definition of a modified strain making straightforward the use of standard strain-driven constitutive laws. At the same time, the continuity of the volumetric strain across multimaterial interfaces can be naturally accepted as a sort of kinematic constraint (stresses can still remain discontinuous across material interfaces). The new element also opens the door to the use of anisotropic constitutive laws, which are typically problematic in the context of mixed elements.

*Corresponding author
Email addresses: rrossi@cimne.upc.edu (R. Rossi), rzorrilla@cimne.upc.edu (R. Zorrilla), ramon.codina@upc.edu (R. Codina)

Keywords: Finite elements, Mixed formulation, anisotropic, Volumetric strain, Nearly incompressible materials, Variational multiscales

1. Motivation

The development of mixed Q_1/Q_1 (multi-linear/multi-linear) and P_1/P_1 (linear/linear) displacement-pressure approaches [1] has represented a milestone in the finite element (FE) technology, opening for the first time the possibility of improving the accuracy of low order meshes while guaranteeing a lock-free behaviour at the nearly-incompressible limit. The key idea of displacement-pressure ($\mathbf{u}$-p) approaches is to split the constitutive response into its deviatoric and volumetric parts. The deviatoric part of the strain is then recovered from the displacement field and fed to the constitutive law which then returns the corresponding deviatoric stress. The volumetric part on the other hand is obtained in terms of the nodal pressure field. Even though this approach effectively solves any volumetric locking issue, it also implies that the total strain is never explicitly computed (in the FE implementation, only deviatoric strain and pressure are available at the Gauss points). The practical downside of this situation is that one cannot make use of standard strain-driven constitutive laws, which represents a practical blocker in the context of commercial codes which need to leverage large material libraries. The proposed approach sidesteps this difficulty by *choosing as primal variable the volumetric strain ε^v instead of the pressure*. In the implementation, the difference is that the total strain can be recovered at the Gauss point level by simply summing the deviatoric part (obtained as before in terms of the displacement gradient) and the volumetric one obtained by interpolation of ε^v. The use of standard constitutive models becomes thus straightforward, effectively resolving the problem described.

A second well known difficulty, which is intrinsic to the use of equal-order, mixed, displacement-pressure fields, is that the pressure is treated as a continuous FE variable. This becomes problematic when multiple materials need to be considered within the domain, since in presence of pressure discontinuities continuous approximations typically manifest unwanted oscillations. Although this can be remedied for example by doubling the pressure degrees of freedom at the interface, [2], such approach is normally inconvenient when more than two materials are present. The use of a continuous discretization for ε^v on the contrary does not prevent discontinuous pressures to rise across the material interface, thus effectively sidestepping such difficulty.

Interestingly, for isotropic linear constitutive relations the proposed formulation can be understood simply as a change of variable with respect to displacement-pressure approaches. When considered in this context, the $\mathbf{u}$-ε^v formulation inherits all the stability properties of the original $\mathbf{u}$-p approach (see e.g. [3] for a recent discussion).

We shall also remark that the use of displacement-strain (total strain) formulations has been proposed previously in [4] as an alternative to the displacement-stress approach, also described in [4]. An enhanced three field formulation (displacement-strain-pressure) $\mathbf{u}$-$\boldsymbol{\varepsilon}$-p has been not long ago proposed in [5]. To the best of our knowledge however this is the first time where a $\mathbf{u}$-ε^v formulation is discussed in detail. To this end, the paper is structured as follows: a mixed displacement-volumetric strain formulation for small strain elasticity is derived as a special case of the displacement-strain formulation in Section 2, where the problem is set at the continuous level and a FE discretisation is proposed. The case of anisotropic materials is studied in Section 3, retrofitting the original formulation to allow the solution of anisotropic problems. This is accomplished by a redefinition of the modified volumetric strain which accounts for the anisotropic behaviour of the material. The article is concluded by a set of convergence tests in Section 4, performed both in the isotropic and anisotropic cases, and by a number of test examples proving the performance of the proposed formulation. Finally, the last section collects the conclusion and further work lines of the paper.

The $\mathbf{u}$-ε^v formulation we propose is implemented and ready to use whitin the open source Kratos Multiphysics framework [6, 7].

2. Formulation

2.1. Governing equations

The essence of the proposed formulation is to modify the (small) strain definition to avoid volumetric locking. This is accomplished by employing a mixed formulation in which the volumetric strain ε^v is considered as an unknown, and interpolated as such when the problem is approximated using finite elements. The key idea is that the standard deviatoric-isochoric splitting is performed at the strain level. The deviatoric part is then computed in terms of the displacements while the isochoric one is expressed in terms

of ε^v. This is expressed in symbols as

$$\boldsymbol{\varepsilon}(\mathbf{x}) = \underbrace{\nabla^s \mathbf{u} - \frac{1}{\alpha}\nabla \cdot \mathbf{u}\mathbf{I}}_{\boldsymbol{\varepsilon}_{\text{dev}}} + \underbrace{\frac{1}{\alpha}\varepsilon^v \mathbf{I}}_{\boldsymbol{\varepsilon}_{\text{iso}}} \tag{1}$$

where $\mathbf{I}$ is the identity matrix. The coefficient α is taken here as $\alpha = 3$ in the 3D case and $\alpha = 2$ in the 2D one. This choice implies that in 2D cases the "volumetric" strain should be understood *as a measure of the area change in the plane* rather than a measure of the real volume change.

Once the strain splitting is defined, the equilibrium problem can be written as

$$-\nabla \cdot \boldsymbol{\sigma}(\boldsymbol{\varepsilon}) = \mathbf{f} \tag{2a}$$

$$\nabla \cdot \mathbf{u} - \varepsilon^v = 0 \tag{2b}$$

where the first equation is the classical equilibrium condition and the second expresses the kinematic relation between the volume variation and the displacement field, which is exact in the continuum for the small deformation case.

No assumption is made up to this point about the constitutive behaviour other than $\boldsymbol{\sigma} = \boldsymbol{\sigma}(\boldsymbol{\varepsilon})$. Likewise, the introduction of the volumetric strain as a variable can be done both for stationary and time dependent problems, although we will restrict ourselves to the former in this paper.

Furthermore, we note that Eq. 2b can be written in incremental form as

$$\nabla \cdot \Delta\mathbf{u} - \Delta\varepsilon^v = 0 \tag{3}$$

$\Delta(\cdot)$ denoting an increment; this choice is completely equivalent to Eq. 2b in the linear case but has some practical advantages in the application of initial conditions or initial guesses of iterative schemes.

2.2. Variational approach

Obtaining a symmetric variational form for the problem described in Eqs. 2a and 2b is not obvious. Our approach for doing so is to begin by considering the mixed displacement-strain form, described in [4] or for the explicit case in [8, 9].

2.2.1. Standard $\mathbf{u}$-$\boldsymbol{\varepsilon}$ *formulation*

Let us start considering the differential form of the $\mathbf{u} - \boldsymbol{\varepsilon}$ formulation, which reads:

$$-\nabla \cdot \mathbb{C} : \boldsymbol{\varepsilon} = \mathbf{f}$$
$$\mathbb{C} : \boldsymbol{\varepsilon} - \mathbb{C} : \nabla^s \mathbf{u} = \mathbf{0}$$

where $\mathbb{C}$ is the constitutive tensor and $\mathbf{f}$ the vector of external body forces. To simplify the exposition, let us consider homogeneous Dirichlet boundary conditions $\mathbf{u} = \mathbf{0}$ on the whole boundary $\partial\Omega$ of the domain Ω where the problem is posed.

Let $\boldsymbol{\delta}_\mathbf{u}$ be the displacement test function (vanishing on $\partial\Omega$) and $\boldsymbol{\delta}_{\boldsymbol{\varepsilon}}$ the strain test function. The weak form of the problem consists of finding $\mathbf{u}$ and $\boldsymbol{\varepsilon}$ in the appropriate spaces such that

$$\int_\Omega \nabla^s \boldsymbol{\delta}_\mathbf{u} : \mathbb{C} : \boldsymbol{\varepsilon} = \int_\Omega \boldsymbol{\delta}_\mathbf{u} \cdot \mathbf{f} \tag{4a}$$

$$-\int_\Omega \boldsymbol{\delta}_{\boldsymbol{\varepsilon}} : \mathbb{C} : (\boldsymbol{\varepsilon} - \nabla^s \mathbf{u}) = 0 \tag{4b}$$

for all test functions $\boldsymbol{\delta}_\mathbf{u}$ and $\boldsymbol{\delta}_{\boldsymbol{\varepsilon}}$. The problem can also be written in the form

$$B_{\mathbf{u}\boldsymbol{\varepsilon}}(\mathbf{u}, \boldsymbol{\varepsilon}; \boldsymbol{\delta}_\mathbf{u}, \boldsymbol{\delta}_{\boldsymbol{\varepsilon}}) := \int_\Omega \nabla^s \boldsymbol{\delta}_\mathbf{u} : \mathbb{C} : \boldsymbol{\varepsilon} - \int_\Omega \boldsymbol{\delta}_{\boldsymbol{\varepsilon}} : \mathbb{C} : (\boldsymbol{\varepsilon} - \nabla^s \mathbf{u}) = \int_\Omega \boldsymbol{\delta}_\mathbf{u} \cdot \mathbf{f} \tag{5}$$

It is observed that the bilinear form $B_{\mathbf{u}\boldsymbol{\varepsilon}}$ is semi-definite:

$$B_{\mathbf{u}\boldsymbol{\varepsilon}}(\mathbf{u}, \boldsymbol{\varepsilon}; \mathbf{u}, -\boldsymbol{\varepsilon}) = \int_\Omega \boldsymbol{\varepsilon} : \mathbb{C} : \boldsymbol{\varepsilon}$$

From this one can easily get a stability estimate for the strain, but not for the displacement. An inf-sup condition is required to bound it in the continuous case which needs to be inherited by the FE interpolation, unless a stabilised FE method is employed. A similar comment applies to the formulation to be proposed later.

If we introduce the functional

$$\mathcal{E}_{\mathbf{u}\boldsymbol{\varepsilon}}(\mathbf{u}, \boldsymbol{\varepsilon}) = \frac{1}{2}\int_\Omega (\boldsymbol{\varepsilon} - \nabla^s \mathbf{u}) : \mathbb{C} : (\boldsymbol{\varepsilon} - \nabla^s \mathbf{u}) - \frac{1}{2}\int_\Omega \nabla^s \mathbf{u} : \mathbb{C} : \nabla^s \mathbf{u} + \int_\Omega \mathbf{u} \cdot \mathbf{f}$$

it is easily seen that Eqs. 4 are precisely its stationary conditions. The way we have written $\mathcal{E}_{\mathbf{u}\boldsymbol{\varepsilon}}$ is intended to motivate the following formulation.

102 *2.2.2.* $\mathbf{u}$-ε^v *formulation*

Our proposal is to start from the variational form of the $\mathbf{u}$-$\boldsymbol{\varepsilon}$ formulation and to substitute the strain formula $\boldsymbol{\varepsilon} := \nabla^s\mathbf{u} - \frac{1}{\alpha}\nabla\cdot\mathbf{u}\mathbf{I} + \frac{1}{\alpha}\varepsilon^v\mathbf{I}$ into it. Thus, let us consider the functional

$$\mathcal{E}_{\mathbf{u}\varepsilon^v}(\mathbf{u},\varepsilon^v) = \frac{1}{2}\frac{1}{\alpha^2}\int_\Omega (\varepsilon^v - \nabla\cdot\mathbf{u})\mathbf{I} : \mathbb{C} : \mathbf{I}(\varepsilon^v - \nabla\cdot\mathbf{u}) - \frac{1}{2}\int_\Omega \nabla^s\mathbf{u} : \mathbb{C} : \nabla^s\mathbf{u} + \int_\Omega \mathbf{u}\cdot\mathbf{f} \tag{6}$$

Let us call

$$\kappa := \frac{1}{\alpha^2}\mathbf{I} : \mathbb{C} : \mathbf{I} \tag{7}$$

which coincides with the volumetric modulus for isotropic materials. It allows us to write the stationary conditions of the functional in Eq. 6 as

$$B_{\mathbf{u}\varepsilon^v}(\mathbf{u},\varepsilon^v;\boldsymbol{\delta}_\mathbf{u},\delta_{\varepsilon^v}) := \int_\Omega (\delta_{\varepsilon^v} - \nabla\cdot\boldsymbol{\delta}_\mathbf{u})\kappa(\varepsilon^v - \nabla\cdot\mathbf{u}) - \int_\Omega \nabla^s\boldsymbol{\delta}_\mathbf{u} : \mathbb{C} : \nabla^s\mathbf{u} = -\int_\Omega \boldsymbol{\delta}_\mathbf{u}\cdot\mathbf{f} \tag{8}$$

for all test functions $\boldsymbol{\delta}_\mathbf{u}$, δ_{ε^v}, where $B_{\mathbf{u}\varepsilon^v}$ is the counterpart of the bilinear form $B_{\mathbf{u}\boldsymbol{\varepsilon}}$ in Eq. 5 for the formulation we propose. Problem 8 can also be split as

$$\int_\Omega \nabla^s\boldsymbol{\delta}_\mathbf{u} : \mathbb{C} : \nabla^s\mathbf{u} + \int_\Omega \nabla\cdot\boldsymbol{\delta}_\mathbf{u}\,\kappa(\varepsilon^v - \nabla\cdot\mathbf{u}) = \int_\Omega \boldsymbol{\delta}_\mathbf{u}\cdot\mathbf{f} \tag{9a}$$

$$\int_\Omega \delta_{\varepsilon^v}\kappa(\varepsilon^v - \nabla\cdot\mathbf{u}) = 0 \tag{9b}$$

for all test functions $\boldsymbol{\delta}_\mathbf{u}$, δ_{ε^v}, which is the counterpart of Problem 4 for the $\mathbf{u}$-ε^v formulation. The strong (differential) form of these equations (for κ constant) is:

$$-\nabla\cdot\mathbb{C} : \nabla^s\mathbf{u} - \kappa\nabla(\varepsilon^v - \nabla\cdot\mathbf{u}) = \mathbf{f} \tag{10a}$$

$$\varepsilon^v - \nabla\cdot\mathbf{u} = 0 \tag{10b}$$

103 Recall that zero Dirichlet conditions have been assumed throughout.

Remark 1. In the case of arbitrary stress-strain relations, Problem 9 can be modified by replacing $\mathbb{C} : \nabla^s \mathbf{u}$ by the stress $\boldsymbol{\sigma}(\boldsymbol{\varepsilon})$ and introducing a scaling physical parameter $\tilde{\kappa}$ (with the same units as κ), so that the variational form of the problem would be

$$\int_\Omega \nabla^s \boldsymbol{\delta}_\mathbf{u} : \boldsymbol{\sigma}(\boldsymbol{\varepsilon}) + \int_\Omega \nabla \cdot \boldsymbol{\delta}_\mathbf{u}\, \tilde{\kappa}(\varepsilon^v - \nabla \cdot \mathbf{u}) = \int_\Omega \boldsymbol{\delta}_\mathbf{u} \cdot \mathbf{f} \tag{11a}$$

$$\int_\Omega \delta_{\varepsilon^v} \tilde{\kappa}(\varepsilon^v - \nabla \cdot \mathbf{u}) = 0 \tag{11b}$$

for all test functions $\boldsymbol{\delta}_\mathbf{u}$ and δ_{ε^v}. □

Remark 2. Even though no assumption on $\mathbb{C}$ has been stated to obtain Problem 9, we will use it for isotropic materials; the way we deal with anisotropic cases is explained in Section 3. Consider then an isotropic material, and let us introduce Π_{dev} as the projection of second order tensors onto their deviatoric component. We may write Eq. 10a as

$$-\nabla \cdot \Pi_{\text{dev}}(\mathbb{C} : \nabla^s \mathbf{u}) - \frac{1}{\alpha} \nabla \cdot (\nabla \cdot \mathbf{u}\, \mathbb{C} : \mathbf{I}) - \kappa \nabla(\varepsilon^v - \nabla \cdot \mathbf{u}) = \mathbf{f} \tag{12}$$

For isotropic materials

$$\frac{1}{\alpha} \nabla \cdot (\nabla \cdot \mathbf{u}\, \mathbb{C} : \mathbf{I}) = \kappa \nabla(\nabla \cdot \mathbf{u})$$

and then Eq. 12 can be written as

$$-\nabla \cdot \Pi_{\text{dev}}(\mathbb{C} : \nabla^s \mathbf{u}) - \kappa \nabla \varepsilon^v = \mathbf{f}$$

The change of variable $p = \kappa \varepsilon^v$ yields the classical $\mathbf{u}$-p formulation of linear elasticity, which would allow us to deal with purely incompressible materials, i.e., $\kappa = \infty$. In this case, Eq. 10b would be $\nabla \cdot \mathbf{u} = 0$. □

Remark 3. In line with the previous remark, let us notice that for anisotropic materials the incompressibility condition $\nabla \cdot \mathbf{u} = 0$ is *not* implied by any limit value of a physical property, as in the isotropic case, but by different conditions that relate the physical properties of an anisotropic material (see for example [10, 11]). □

2.3. Variational Multi-Scale stabilisation

Let us consider the continuous problem given in Eq. 8. The bilinear form of the problem satisfies:

$$B_{\mathbf{u}\varepsilon^v}(\mathbf{u},\varepsilon^v;-\mathbf{u},\varepsilon^v) = \int_\Omega \kappa(\varepsilon^v)^2 - \int_\Omega \kappa(\nabla\cdot\mathbf{u})^2 + \int_\Omega \nabla^s\mathbf{u} : \mathbb{C} : \nabla^s\mathbf{u} \quad (13)$$

For isotropic materials, the second term is precisely the volumetric component of the third one and, since the deviatoric and volumetric components of a tensor are orthogonal, we are left with only the deviatoric part. In the case of anisotropic or nonlinear materials, the scaling coefficient $\tilde{\kappa}$ should be chosen such that the second term could be absorbed by the third one. In any case, it is observed that this expression provides control on the deviatoric part of $\nabla^s\mathbf{u}$ and on ε^v. Thus, we miss control on the volumetric part of $\nabla^s\mathbf{u}$, which at the continuous level can be obtained from an inf-sup condition from the control on ε^v. However, if we use the standard Galerkin FE discretisation, this inf-sup condition will not necessarily hold. Moreover, since derivatives of ε^v do not appear in Eq. 13, there is no guarantee to have them bounded, and the FE approximation to this variable may display node-to-node oscillations. This effect is particularly important in materials close to incompressible, case in which $\varepsilon^v \to 0$ and, even if $\kappa \to \infty$, $\kappa(\varepsilon^v)^2 \to 0$ (since $\kappa\varepsilon^v$ must remain bounded).

In our numerical experiments we have observed that the Galerkin approximation to the problem in Eq. 8 is polluted by strong numerical oscillations. This is why we present now a stabilised FE formulation based on the Variational Multi-Scale (VMS) concept [12, 13].

Let us consider the domain Ω discretised in a partition $\{\Omega^e\}$ of elements of characteristic size h, index e ranging from 1 to the total number of elements. From this, we may construct the interpolating spaces for $\mathbf{u}$ and ε^v; standard continuous Lagrangian interpolations will be assumed for both variables. FE functions will be identified with the subscript h.

The VMS method is based on the separation of the unknown fields, in this case the displacement $\mathbf{u}$ and the volumetric strain ε^v, in two scales. On one hand we have the scale which can be represented by the FE solution, $\mathbf{u}_h$ and ε^v_h. On the other hand we have the so called sub-scales, which represent the part of the solution that cannot be captured by the FE mesh and needs to be modelled. The sub-scales are denoted with the subindex s, as $\mathbf{u}_s$ and ε^v_s. We thus have the decomposition

$$\mathbf{u} = \mathbf{u}_h + \mathbf{u}_s \quad (14a)$$

$$\varepsilon^v = \varepsilon_h^v + \varepsilon_s^v \tag{14b}$$

A similar splitting holds for the test functions, yielding the equation in the FE space and in the space of sub-scales. The idea is now to insert these splittings into the variational form of the problem, integrate by parts terms involving derivatives of the sub-scales and then give an approximation for them (not for their derivatives).

Let us consider then Problem 9 taking the test functions in the corresponding FE spaces, using the splittings in Eqs. 14 and integrating by parts within each element. The result is:

$$\begin{aligned}
&\int_\Omega \nabla^s \boldsymbol{\delta}_{\mathbf{u}_h} : \mathbb{C} : \nabla^s \mathbf{u}_h - \sum_e \int_{\Omega^e} \mathbf{u}_s \cdot \nabla \cdot \mathbb{C} : \nabla^s \boldsymbol{\delta}_{\mathbf{u}_h} \\
&\quad + \int_\Omega \nabla \cdot \boldsymbol{\delta}_{\mathbf{u}_h} \, \kappa \, (\varepsilon_h^v + \varepsilon_s^v - \nabla \cdot \mathbf{u}_h) + \sum_e \int_{\Omega^e} \mathbf{u}_s \cdot \kappa \nabla \nabla \cdot \boldsymbol{\delta}_{\mathbf{u}_h} \\
&\quad = \int_\Omega \boldsymbol{\delta}_{\mathbf{u}_h} \cdot \mathbf{f}
\end{aligned} \tag{15a}$$

$$\int_\Omega \delta_{\varepsilon_h^v} \kappa (\varepsilon_h^v + \varepsilon_s^v - \nabla \cdot \mathbf{u}_h) + \sum_e \int_{\Omega^e} \mathbf{u}_s \cdot \kappa \nabla \delta_{\varepsilon_h^v} = 0 \tag{15b}$$

where sub-scales on the element boundaries have been discarded, although this assumption can be relaxed [14]. Writing Eqs. 15 together we have:

$$\begin{aligned}
&\int_\Omega \nabla^s \boldsymbol{\delta}_{\mathbf{u}_h} : \mathbb{C} : \nabla^s \mathbf{u}_h + \int_\Omega (\delta_{\varepsilon_h^v} + \nabla \cdot \boldsymbol{\delta}_{\mathbf{u}_h}) \, \kappa \, (\varepsilon_h^v - \nabla \cdot \mathbf{u}_h) \\
&\quad + \sum_e \int_{\Omega^e} \mathbf{u}_s \cdot [-\nabla \cdot \mathbb{C} : \nabla^s \boldsymbol{\delta}_{\mathbf{u}_h} + \kappa \nabla (\varepsilon_h^v + \nabla \cdot \boldsymbol{\delta}_{\mathbf{u}_h})] \\
&\quad + \sum_e \int_{\Omega^e} \varepsilon_s^v \, \kappa \, (\delta_{\varepsilon_h^v} + \nabla \cdot \boldsymbol{\delta}_{\mathbf{u}_h}) = \int_\Omega \boldsymbol{\delta}_{\mathbf{u}_h} \cdot \mathbf{f}
\end{aligned} \tag{16}$$

The model is completed by the choice of an approximation for the sub-scales. The counterpart of Eq. 16 with the test functions taken in the space of sub-scales would lead to an equation projected onto this space stating that the differential operator of the problem is equal to the residual of the FE scales. This operator applied to the sub-scales can then be approximated by a diagonal matrix using different arguments (see [13] for a review and details). In view of the equations to be solved 10, the final result is:

$$\mathbf{u}_s = \tau_1 P_s [\mathbf{f} + \nabla \cdot \mathbb{C} : \nabla^s \mathbf{u}_h + \kappa \nabla (\varepsilon_h^v - \nabla \cdot \mathbf{u}_h)] \tag{17a}$$

$$\varepsilon_s^v = \tau_2 P_s[\nabla \cdot \mathbf{u}_h - \varepsilon_h^v] \tag{17b}$$

where τ_1 and τ_2 are the stabilisation parameters, given below, and P_s is the projection onto the space of sub-scales, either of $\mathbf{u}_s$ or of ε_s^v.

Inserting the sub-scales given by Eqs. 17 into Eq. 16 we finally obtain the stabilised FE method we propose, which consists in finding $\mathbf{u}_h$ and ε_h^v such that

$$\begin{aligned}
&B_{\mathbf{u}\varepsilon^v,\mathrm{stab}}(\mathbf{u}_h, \varepsilon_h^v; \boldsymbol{\delta}_{\mathbf{u}_h}, \delta_{\varepsilon_h^v}) \\
&:= \int_\Omega \nabla^s \boldsymbol{\delta}_{\mathbf{u}_h} : \mathbb{C} : \nabla^s \mathbf{u}_h + \int_\Omega (\delta_{\varepsilon_h^v} + \nabla \cdot \boldsymbol{\delta}_{\mathbf{u}_h})\, \kappa\, (\varepsilon_h^v - \nabla \cdot \mathbf{u}_h) \\
&\quad + \sum_e \int_{\Omega^e} \tau_1 P_s[\nabla \cdot \mathbb{C} : \nabla^s \mathbf{u}_h + \kappa \nabla(\varepsilon_h^v - \nabla \cdot \mathbf{u}_h)] \\
&\qquad\qquad \cdot [-\nabla \cdot \mathbb{C} : \nabla^s \boldsymbol{\delta}_{\mathbf{u}_h} + \kappa \nabla(\delta_{\varepsilon_h^v} + \nabla \cdot \boldsymbol{\delta}_{\mathbf{u}_h})] \\
&\quad + \sum_e \int_{\Omega^e} \tau_2 P_s(\nabla \cdot \mathbf{u}_h - \varepsilon_h^v) \kappa\, (\delta_{\varepsilon_h^v} + \nabla \cdot \boldsymbol{\delta}_{\mathbf{u}_h}) \\
&\quad = \int_\Omega \boldsymbol{\delta}_{\mathbf{u}_h} \cdot \mathbf{f} - \sum_e \int_{\Omega^e} \tau_1 P_s[\mathbf{f}] \cdot [-\nabla \cdot \mathbb{C} : \nabla^s \boldsymbol{\delta}_{\mathbf{u}_h} + \kappa \nabla(\delta_{\varepsilon_h^v} + \nabla \cdot \boldsymbol{\delta}_{\mathbf{u}_h})] \\
&\quad =: L_{\mathbf{u}\varepsilon^v,\mathrm{stab}}(\boldsymbol{\delta}_{\mathbf{u}_h}, \delta_{\varepsilon_h^v})
\end{aligned} \tag{18}$$

for all test functions $\boldsymbol{\delta}_{\mathbf{u}_h}$ and $\delta_{\varepsilon_h^v}$.

To complete the definition of the method, we need to define the projection P_s and the expression of stabilisation parameters. Even though the space for the sub-scales can be defined in different manners (bubble functions, approximation to Green's function,...) when arriving to Eq. 17 there are essentially two options, namely, to take the space of sub-scale as the space of FE residuals, yielding $P_s = I$ (the identity) or to take it as L^2 orthogonal to the FE space, case in which P_s is the orthogonal projection to this space. The second option has theoretical and practical advantages, as reported for example in [4, 15, 16, 17]. However, here we will consider the most common option of taking $P_s = I$, leading to classical residual-based stabilised FE methods. See also [13] for further discussion.

Regarding the stabilisation parameters, they can be determined by scaling arguments or by assuming that the sub-scales are bubble functions. In either case, the result is that they should behave as

$$\tau_1 = c_1 \frac{h^2}{G}, \quad \tau_2 = c_2 \frac{G}{G + \kappa} \tag{19}$$

where G an equivalent effective shear modulus and c_1 and c_2 are algorithmic constants, that in the case of linear elements we take as $c_1 = 2$, $c_2 = 4$. Let us remark that the definition of "equivalent effective shear modulus" is not univocal in the context of anisotropic materials. We defer the discussion on the exact definition of such term to the following sections.

The formulation we propose is given by Eq. 18 with $P_s = I$ and τ_1 and τ_2 given in Eq. 19. Let us consider the case of linear elements, in which second derivatives inside the elements are zero. Eq. 18 can then be arranged to give

$$\begin{aligned} &B_{\mathbf{u}\varepsilon^v,\text{stab,lin}}(\mathbf{u}_h, \varepsilon_h^v; \boldsymbol{\delta}_{\mathbf{u}_h}, \delta_{\varepsilon_h^v}) \\ &:= \int_\Omega \nabla^s \boldsymbol{\delta}_{\mathbf{u}_h} : \mathbb{C} : \nabla^s \mathbf{u}_h + \int_\Omega (1-\tau_2)(\delta_{\varepsilon_h^v} + \nabla \cdot \boldsymbol{\delta}_{\mathbf{u}_h})\, \kappa\, (\varepsilon_h^v - \nabla \cdot \mathbf{u}_h) \\ &\quad + \int_\Omega \tau_1 \kappa^2 \nabla \delta_{\varepsilon_h^v} \cdot \nabla \varepsilon_h^v = \int_\Omega \boldsymbol{\delta}_{\mathbf{u}_h} \cdot \mathbf{f} - \int_\Omega \tau_1 \mathbf{f} \cdot \kappa \nabla \delta_{\varepsilon_h^v} \end{aligned} \tag{20}$$

Remark 4. Even though it is not the purpose of this paper to analyse the stability and convergence properties of the method in detail, the simplified problem in Eq. 20 allows us to understand the effect on stability of τ_1 and τ_2. Assuming these for simplicity to be constant, we have that

$$\begin{aligned} B_{\mathbf{u}\varepsilon^v,\text{stab,lin}}(\mathbf{u}_h, \varepsilon_h^v; \mathbf{u}_h, \varepsilon_h^v) &= \|\mathbb{C}^{1/2} : \nabla^s \mathbf{u}_h\|^2 + (1-\tau_2)\|\kappa^{1/2} \varepsilon_h^v\|^2 \\ &\quad - (1-\tau_2)\|\kappa^{1/2} \nabla \cdot \mathbf{u}_h\|^2 + \tau_1 \|\kappa \nabla \delta_{\varepsilon_h^v}\|^2 \end{aligned}$$

where $\mathbb{C}^{1/2}$ is the square root of the positive-definite tensor $\mathbb{C}$ and $\|\cdot\|$ is the L^2 norm in Ω. From this expression we observe that

- τ_2 reduces the (positive) L^2 control on ε_h^v.
- τ_2 reduces the subtracting L^2 norm of $\nabla \cdot \mathbf{u}_h$.
- τ_1 provides control on the derivatives of ε_h^v.

It is observed that the crucial parameter from the numerical point of view is τ_1 and that we need to ensure that $\tau_2 < 1$. □

Remark 5. In order to be able to use generic materials we may proceed as indicated in Remark 1. If $\tilde{\kappa}$ is an adequate scaling physical parameter, the problem to be solved for a general constitutive law $\boldsymbol{\sigma} = \boldsymbol{\sigma}(\boldsymbol{\varepsilon})$ is

$$\int_\Omega \nabla^s \boldsymbol{\delta}_{\mathbf{u}_h} : \boldsymbol{\sigma}(\boldsymbol{\varepsilon}_h) + \int_\Omega (1-\tau_2)(\delta_{\varepsilon_h^v} + \nabla \cdot \boldsymbol{\delta}_{\mathbf{u}_h})\, \tilde{\kappa}\, (\varepsilon_h^v - \nabla \cdot \mathbf{u}_h)$$

$$+\int_\Omega \tau_1 \tilde{\kappa}^2 \nabla\delta_{\varepsilon_h^v}\cdot\nabla\varepsilon_h^v = \int_\Omega \boldsymbol{\delta}_{\mathbf{u}_h}\cdot\mathbf{f} - \int_\Omega \tau_1 \mathbf{f}\cdot\tilde{\kappa}\nabla\delta_{\varepsilon_h^v} \tag{21}$$

We remark here that the stabilization factor τ_2 does not enter in the definition of the FE strain $\boldsymbol{\varepsilon}_h$, and is hence not employed in the calculation of the stress.

The formulation given by Eq. 21 reduces to the linear one when one uses the strain $\boldsymbol{\varepsilon}_h = \nabla^s\mathbf{u}_h$ in the constitutive law. A dfferent choice is to use instead the modified strain (following the, admittedly heuristic, rationale that such strain is "better" at the Gauss point level)

$$\boldsymbol{\varepsilon}_h := \nabla^s\mathbf{u}_h - \frac{1}{\alpha}\nabla\cdot\mathbf{u}_h\,\mathbf{I} + \frac{1}{\alpha}\varepsilon_h^v\mathbf{I} \tag{22}$$

Should this be the case, the first term in Eq. 21 becomes

$$\int_\Omega \nabla^s\boldsymbol{\delta}_{\mathbf{u}_h} : \left[\boldsymbol{\sigma}(\boldsymbol{\varepsilon}_h) - \mathbb{C} : \left(-\frac{1}{\alpha}\nabla\cdot\mathbf{u}_h\,\mathbf{I} + \frac{1}{\alpha}\varepsilon_h^v\mathbf{I}\right)\right] \tag{23}$$

where $\mathbb{C} := \left.\frac{\partial\boldsymbol{\sigma}}{\partial\boldsymbol{\varepsilon}_h}\right|_{\boldsymbol{\varepsilon}_h}$ should be interpreted as the tangent constitutive tensor of the constitutive law.

As we will show later, the tangent matrix of a Newton-Raphson linearisation of the problem in Eq. 21 using $\boldsymbol{\varepsilon}_h = \nabla^s\mathbf{u}_h$ is identical to the one obtained using the modification in Eq. 23 with the strain given by Eq. 22, although the residual would of course be different. In our numerical examples we have employed the modification in Eq. 23, although similar results are expected when this modification is not done. □

2.4. Finite Element Implementation—Isotropic case

A number of, rather standard, definitions are useful to write the FE discretisation of the proposed discrete variational problem 21. Let N_I be the standard (Lagrangian) shape function of node I of the FE mesh, and x, y, z the Cartesian coordinates, and let us introduce the following arrays, whose definition depends on the number of space dimensions:

$$\mathbf{B}_I = \begin{pmatrix} \frac{\partial N_I}{\partial x} & 0 & 0 \\ 0 & \frac{\partial N_I}{\partial y} & 0 \\ 0 & 0 & \frac{\partial N_I}{\partial x} \\ \frac{\partial N_I}{\partial y} & \frac{\partial N_I}{\partial x} & 0 \\ 0 & \frac{\partial N_I}{\partial z} & \frac{\partial N_I}{\partial y} \\ \frac{\partial N_I}{\partial z} & 0 & \frac{\partial N_I}{\partial x} \end{pmatrix} \ (3D)\ ,\ \mathbf{B}_I = \begin{pmatrix} \frac{\partial N_I}{\partial x} & 0 \\ 0 & \frac{\partial N_I}{\partial y} \\ \frac{\partial N_I}{\partial y} & \frac{\partial N_I}{\partial x} \end{pmatrix} \ (2D) \tag{24}$$

$$\mathbf{m} := \begin{pmatrix} 1 \\ 1 \\ 1 \\ 0 \\ 0 \\ 0 \end{pmatrix} \ (3D) \ , \ \mathbf{m} := \begin{pmatrix} 1 \\ 1 \\ 0 \end{pmatrix} \ (2D) \tag{25}$$

$$\mathbf{G}_I := \begin{pmatrix} \frac{\partial N_I}{\partial x} \\ \frac{\partial N_I}{\partial y} \\ \frac{\partial N_I}{\partial z} \end{pmatrix} \ (3D) \ , \ \mathbf{G}_I := \begin{pmatrix} \frac{\partial N_I}{\partial x} \\ \frac{\partial N_I}{\partial y} \end{pmatrix} \ (2D) \tag{26}$$

$$\mathbf{P} := \mathbf{I} - \frac{1}{\alpha}\mathbf{m}\mathbf{m}^{\mathbf{t}} \tag{27}$$

$$\kappa := \frac{\mathbf{m}^{\mathbf{t}}\mathbf{C}\mathbf{m}}{\alpha^2} \tag{28}$$

where $\mathbf{C}$ is the Voigt representation of the tangent constitutive tensor $\mathbb{C} := \left.\frac{\partial \boldsymbol{\sigma}}{\partial \boldsymbol{\varepsilon}_h}\right|_{\boldsymbol{\varepsilon}_h}$.

The FE residual assumes finally a slightly different form depending on the choice of $\boldsymbol{\varepsilon}_h$ (see Remark 5). Namely if we choose $\boldsymbol{\varepsilon}_h := \nabla^s \mathbf{u}_h - \frac{1}{\alpha}\nabla\cdot\mathbf{u}_h\,\mathbf{I} + \frac{1}{\alpha}\varepsilon_h^v\mathbf{I}$ (option we followed in our implementation) the residual is

$$\mathbf{R}_I := \begin{pmatrix} N_I\mathbf{f} - \mathbf{B}_I^t\boldsymbol{\sigma}(\boldsymbol{\varepsilon}_h) + \frac{1}{\alpha}\mathbf{B}_I^t\mathbf{C}\mathbf{m}\left(N_J\varepsilon_{h\,J}^v - \mathbf{G}_J^t\mathbf{u}_{h\,J}\right) - (1-\tau_2)\,\kappa\mathbf{G}_I\left(N_J\varepsilon_{h\,J}^v - \mathbf{G}_J^t\mathbf{u}_{h\,J}\right) \\ (1-\tau_2)\,\kappa N_I\left(N_J\varepsilon_{h\,J}^v - \mathbf{G}_J^t\mathbf{u}_{h\,J}\right) + \kappa^2\mathbf{G}_I^t\tau_1\mathbf{G}_J\varepsilon_{h\,J}^v - \kappa\mathbf{G}_I^t\tau_1\mathbf{f} \end{pmatrix} \tag{29}$$

If instead we choose $\boldsymbol{\varepsilon}_h := \nabla^s\mathbf{u}_h$ the residual simplifies to

$$\mathbf{R}_I := \begin{pmatrix} N_I\mathbf{f} - \mathbf{B}_I^t\boldsymbol{\sigma}(\boldsymbol{\varepsilon}_h) - (1-\tau_2)\,\kappa\mathbf{G}_I\left(N_J\varepsilon_{h\,J}^v - \mathbf{G}_J^t\mathbf{u}_{h\,J}\right) \\ (1-\tau_2)\,\kappa N_I\left(N_J\varepsilon_{h\,J}^v - \mathbf{G}_J^t\mathbf{u}_{h\,J}\right) + \kappa^2\mathbf{G}_I^t\tau_1\mathbf{G}_J\varepsilon_{h\,J}^v - \kappa\mathbf{G}_I^t\tau_1\mathbf{f} \end{pmatrix} \tag{30}$$

The definition of the discrete problem is completed by the Newton–Raphson linearization. The derivative of the stress term can be computed as

$$\begin{aligned} \mathbf{B}_I^t\frac{\partial\boldsymbol{\sigma}(\boldsymbol{\varepsilon})}{\partial\mathbf{u}_{h\,J}} = \mathbf{B}_I^t\frac{\partial\boldsymbol{\sigma}(\boldsymbol{\varepsilon})}{\partial\boldsymbol{\varepsilon}}\frac{\partial\boldsymbol{\varepsilon}}{\partial\mathbf{u}_{h\,J}} = \mathbf{B}_I^t\frac{\partial\boldsymbol{\sigma}(\boldsymbol{\varepsilon})}{\partial\boldsymbol{\varepsilon}}\frac{\partial\left(\nabla^s\mathbf{u}_h - \frac{1}{\alpha}\nabla\cdot\mathbf{u}_h\mathbf{I} + \frac{1}{\alpha}\varepsilon_h^v\mathbf{I}\right)}{\partial\mathbf{u}_{h\,J}} \\ = \mathbf{B}_I^t\mathbf{C}\mathbf{B}_J - \frac{1}{\alpha}\mathbf{B}_I^t\mathbf{C}\mathbf{m}\mathbf{G}_J^t \end{aligned} \tag{31}$$

and

$$\mathbf{B}_I^t \frac{\partial \boldsymbol{\sigma}(\boldsymbol{\varepsilon})}{\partial \varepsilon_{hJ}^v} = \mathbf{B}_I^t \frac{\partial \boldsymbol{\sigma}(\boldsymbol{\varepsilon})}{\partial \boldsymbol{\varepsilon}} \frac{\partial \boldsymbol{\varepsilon}}{\partial \varepsilon_{hJ}^v} = \mathbf{B}_I^t \frac{\partial \boldsymbol{\sigma}(\boldsymbol{\varepsilon})}{\partial \boldsymbol{\varepsilon}} \frac{\partial \left(\nabla^s \mathbf{u}_h - \frac{1}{\alpha}\nabla \cdot \mathbf{u}_h \mathbf{I} + \frac{1}{\alpha}\varepsilon_h^v \mathbf{I}\right)}{\partial \varepsilon_{hJ}^v}$$
$$= \frac{1}{\alpha} \mathbf{B}_I^t \mathbf{C} \mathbf{m} N_J \quad (32)$$

This allows to obtain the tangent operator as

$$\mathbf{LHS}_{IJ} := \begin{pmatrix} \mathbf{B}_I^t \mathbf{C} \mathbf{B}_J - (1-\tau_2)\,\kappa \mathbf{G}_I \mathbf{G}_J^t & (1-\tau_2)\,\kappa \mathbf{G}_I N_J \\ (1-\tau_2)\,\kappa N_I \mathbf{G}_J^t & -(1-\tau_2)\,\kappa N_I N_J - \tau_1 \kappa^2 \mathbf{G}_I^t \mathbf{G}_J \end{pmatrix} \quad (33)$$

providing as expected a symmetric tangent (provided that $\mathbf{C}$ is symmetric).

Remark 6. Note that the same expression of the tangent is obtained independently on the definition of $\boldsymbol{\varepsilon}_h$. We observe however that for a non linear material the actual value of the elasticity tensor (which we recall is defined as $\mathbb{C} := \frac{\partial \boldsymbol{\sigma}}{\partial \boldsymbol{\varepsilon}_h}\Big|_{\boldsymbol{\varepsilon}_h}$) may vary depending on the definition of $\boldsymbol{\varepsilon}_h$, thus finally resulting in a different stiffness. □

3. Anisotropy

The proposed formulation works nicely when the material is approximately isotropic; however, experimentation with strongly anisotropic materials shows that instabilities appear in both the volumetric strain and in the displacement fields. A possibility to address this problem is to try to reduce the anisotropic case to a "similar" isotropic problem, for which the method is known to work good. To this end, we observe that any anisotropic tensor $\mathbb{C}$ can be written as $\mathbb{C} = \mathbb{T}^t : \hat{\mathbb{C}} : \mathbb{T}$ where $\hat{\mathbb{C}}$ is an *isotropic* elasticity tensor. Such property will allow us to propose a slight change in the choice of our modified volumetric strain. The following subsections detail first the construction of the "isotropic mapping" and later introduce the proposed change in the volumetric strain definition.

3.1. Constitutive tensor scaling: the closest isotropic tensor

The property $\mathbb{C} = \mathbb{T}^t : \hat{\mathbb{C}} : \mathbb{T}$ is easily proved constructively. Let us assume that $\mathbf{C}$ and $\hat{\mathbf{C}}$ are the Voigt counterparts of $\mathbb{C}$ and $\hat{\mathbb{C}}$. Such matrices are known to be symmetric and positive definite and hence admit a square root. Thus if we define $\mathbf{c} := \mathbf{C}^{1/2}$ and $\hat{\mathbf{c}} := \hat{\mathbf{C}}^{1/2}$, and we observe that such matrices

are also symmetric, we can write, if we assume that the decomposition exists,

$$\mathbf{C} = \mathbf{c}\mathbf{c} = \mathbf{c}^t\mathbf{c} = \mathbf{T}^t\hat{\mathbf{C}}\mathbf{T} = \mathbf{T}^t\hat{\mathbf{c}}^t\hat{\mathbf{c}}\mathbf{T} \tag{34}$$

implying that

$$\mathbf{c} = \hat{\mathbf{c}}\mathbf{T} \implies \mathbf{T} = \hat{\mathbf{c}}^{-1}\mathbf{c} \tag{35}$$

Even though such decomposition is valid for any choice of $\hat{\mathbf{C}}$, in practice it is important to choose such tensor *as close as possible* to its anisotropic counterpart, so to guarantee that for an initially isotropic material the matrix $\mathbf{T}$ is exactly the identity. Following the ideas in [18] we choose $\hat{\mathbf{C}}$ so to minimize the Frobenius norm $||\mathbf{C}-\hat{\mathbf{C}}||_F$, *with the additional constraint of exactly representing the bulk modulus defined in Eq. 7* of the original anisotropic tensor. This gives rise to the formulas

$$\hat{\mathbf{C}} = 3\left(\frac{\alpha}{3}\kappa\right)\mathbf{J} + 2\mu\mathbf{K} \tag{36}$$

where $\mathbf{J} := \mathbf{t}\mathbf{t}^\mathbf{t}$ and $\mathbf{K} := \mathbf{I_4} - \mathbf{J}$, with $\mathbf{t}$ defined as

$$\mathbf{t} := \begin{pmatrix} \frac{1}{\sqrt{3}} \\ \frac{1}{\sqrt{3}} \\ \frac{1}{\sqrt{3}} \\ 0 \\ 0 \\ 0 \end{pmatrix} \ (3D) \ , \ \mathbf{t} := \begin{pmatrix} \frac{1}{\sqrt{2}} \\ \frac{1}{\sqrt{2}} \\ 0 \end{pmatrix} \ (2D) \tag{37}$$

and

$$\mathbf{I_4} = \begin{pmatrix} 1 & 0 & 0 & 0 & 0 & 0 \\ 0 & 1 & 0 & 0 & 0 & 0 \\ 0 & 0 & 1 & 0 & 0 & 0 \\ 0 & 0 & 0 & 0.5 & 0 & 0 \\ 0 & 0 & 0 & 0 & 0.5 & 0 \\ 0 & 0 & 0 & 0 & 0 & 0.5 \end{pmatrix} \ (3D) \ , \ \mathbf{I_4} = \begin{pmatrix} 1 & 0 & 0 \\ 0 & 1 & 0 \\ 0 & 0 & 0.5 \end{pmatrix} \ (2D) \tag{38}$$

Using Voigt's notation, the bulk modulus κ defined in Eq. 7 and appearing in Eq. 36 is

$$\kappa = \frac{\mathbf{m}^\mathbf{t}\mathbf{C}\mathbf{m}}{\alpha^2} \tag{39}$$

a choice that enforces that *the bulk of the original anisotropic tensor* $\mathbf{C}$ *coincides exactly with the one of the "closest" tensor* $\hat{\mathbf{C}}$.

Under these assumptions, the 1st Lamé parameter μ of the closest isotropic tensor in Eq. 36 can be obtained in closed form from the minimization of the Frobenius error norm $||\mathbf{C} - \hat{\mathbf{C}}||_F$ to give

$$\mu = 0.2(C_{00} - 2C_{01} + C_{11} + C_{22})\,(2D) \tag{40a}$$

$$\mu = \frac{4}{33}\big[C_{00} - C_{01} - C_{02} + C_{11} - C_{12} + C_{22} + \frac{3}{4}(C_{33} + C_{44} + C_{55})\big]\,(3D) \tag{40b}$$

3.2. Variational approach

With the proposed mapping, the mixed strain-displacement problem in Eq. 4a and Eq. 4b becomes

$$\int_\Omega \nabla^s \boldsymbol{\delta}_\mathbf{u} : \mathbb{T}^t : \hat{\mathbb{C}} : \mathbb{T} : \boldsymbol{\varepsilon} = \int_\Omega \boldsymbol{\delta}_\mathbf{u} \cdot \mathbf{f} \tag{41a}$$

$$-\int_\Omega \boldsymbol{\delta}_{\boldsymbol{\varepsilon}} : \mathbb{T}^t : \hat{\mathbb{C}} : \mathbb{T} : (\boldsymbol{\varepsilon} - \nabla^s \mathbf{u}) = 0 \tag{41b}$$

which, once we define $\hat{\boldsymbol{\varepsilon}} := \mathbb{T} : \boldsymbol{\varepsilon}$ (and likewise for the test function) shows an obvious similarity with the isotropic case. The essential idea of our proposal is hence *to modify* $\hat{\boldsymbol{\varepsilon}}$ *instead of* $\boldsymbol{\varepsilon}$ to obtain an equation in terms of the volumetric strain. Doing such exercise we obtain

$$\hat{\boldsymbol{\varepsilon}} = \mathbb{T} : \nabla^s \mathbf{u} - \frac{1}{\alpha}\mathrm{Tr}\left(\mathbb{T} : \nabla^s \mathbf{u}\right)\mathbf{I} + \frac{1}{\alpha}\hat{\varepsilon^v}\mathbf{I}$$

What follows is simply an algebraic exercise to follow the same steps as in the general case, now particularised to the change of variables proposed.

Taking into account that $\mathbb{T}^{-1} : \mathbb{T} = \mathbb{T} : \mathbb{T}^{-1} = \mathbb{I}$ and that the trace can be written as $\mathrm{Tr}\left(\mathbb{T} : \nabla^s \mathbf{u}\right) = \mathbf{I} : \mathbb{T} : \nabla^s \mathbf{u}$, we obtain

$$\hat{\boldsymbol{\varepsilon}} = \mathbb{T} : \nabla^s \mathbf{u} - \frac{\mathbf{I} : \mathbb{T} : \nabla^s \mathbf{u}}{\alpha}\mathbb{T} : \mathbb{T}^{-1} : \mathbf{I} + \frac{\hat{\varepsilon^v}}{\alpha}\mathbb{T} : \mathbb{T}^{-1} : \mathbf{I} \tag{42}$$

Premultiplying by $\mathbb{T}^{-1}$: we can recover the enrichment of the original strain as

$$\boldsymbol{\varepsilon} = \nabla^s \mathbf{u} - \frac{\mathbf{I} : \mathbb{T} : \nabla^s \mathbf{u}}{\alpha}\mathbb{T}^{-1} : \mathbf{I} + \frac{\hat{\varepsilon^v}}{\alpha}\mathbb{T}^{-1} : \mathbf{I} \tag{43}$$

Note that for isotropic materials $\mathbb{T} = \mathbb{I}$, thus implying that the original formulation is recovered.

Once arrived at this point, the derivation follows exactly the same path as in the general case. By substituting Eq. 42 into Eq. 41a and 41b we obtain

$$\int_\Omega \nabla^s \boldsymbol{\delta}_\mathbf{u} : \mathbb{T}^t : \hat{\mathbb{C}} : \left(\mathbb{T} : \nabla^s \mathbf{u} - \frac{\mathbf{I} : \mathbb{T} : \nabla^s \mathbf{u}}{\alpha} \mathbf{I} + \frac{\hat{\varepsilon^v}}{\alpha} \mathbf{I} \right) = \int_\Omega \boldsymbol{\delta}_\mathbf{u} \cdot \mathbf{f}$$

and, proceeding for the strain test function as for the strain,

$$- \int_\Omega \left(\nabla^s \boldsymbol{\delta}_\mathbf{u} : \mathbb{T}^t - \frac{\mathbf{I} : \mathbb{T} : \nabla^s \boldsymbol{\delta}_\mathbf{u}}{\alpha} \mathbf{I} + \frac{\delta_{\hat{\varepsilon^v}}}{\alpha} \mathbf{I} \right) : \hat{\mathbb{C}} : \left(- \frac{\mathbf{I} : \mathbb{T} : \nabla^s \mathbf{u}}{\alpha} \mathbf{I} + \frac{\hat{\varepsilon^v}}{\alpha} \mathbf{I} \right) = 0$$

Substituting $\mathbb{T}^t : \hat{\mathbb{C}} : \mathbb{T}$ by the original $\mathbb{C}$ plus rearranging and collecting the relevant terms we then arrive to

$$\begin{aligned} &\int_\Omega \nabla^s \boldsymbol{\delta}_\mathbf{u} : \mathbb{C} : \nabla^s \mathbf{u} \\ &- \int_\Omega \left(- \frac{\mathbf{I} : \mathbb{T} : \nabla^s \boldsymbol{\delta}_\mathbf{u}}{\alpha} \right) \mathbf{I} : \mathbb{T}^{-t} : \mathbb{C} : \mathbb{T}^{-1} : \mathbf{I} \left(- \frac{\mathbf{I} : \mathbb{T} : \nabla^s \mathbf{u}}{\alpha} + \frac{\hat{\varepsilon^v}}{\alpha} \right) \\ &\qquad = \int_\Omega \boldsymbol{\delta}_\mathbf{u} \cdot \mathbf{f} \qquad (44a) \\ &- \int_\Omega \left(\frac{\delta_{\hat{\varepsilon^v}}}{\alpha} \right) \mathbf{I} : \mathbb{T}^{-t} : \mathbb{C} : \mathbb{T}^{-1} : \mathbf{I} \left(- \frac{\mathbf{I} : \mathbb{T} : \nabla^s \mathbf{u}}{\alpha} + \frac{\hat{\varepsilon^v}}{\alpha} \right) = 0 \qquad (44b) \end{aligned}$$

Unfortunately, the previous form is not fully convenient for the mechanical response modelling as the constitutive law input strain would be $\nabla^s \mathbf{u}$ rather than $\hat{\boldsymbol{\varepsilon}}$. This can be avoided by rearranging the enriched strain definition in Eq. 42 as

$$\nabla^s \mathbf{u} = \mathbb{T}^{-1} : \hat{\boldsymbol{\varepsilon}} - \frac{1}{\alpha} \mathbb{T}^{-1} : \mathbf{I} \left(\hat{\varepsilon^v} - \mathbf{I} : \mathbb{T} : \nabla^s \mathbf{u} \right) \qquad (45)$$

and substituting it into Eq. 44a.

We can now observe that with the proposed choice of "closest isotropic tensor" the equality

$$\hat{\kappa} := \frac{\mathbf{I} : \mathbb{T}^{-t} : \mathbb{C} : \mathbb{T}^{-1} : \mathbf{I}}{\alpha^2} = \frac{\mathbf{I} : \hat{\mathbb{C}} : \mathbf{I}}{\alpha^2} = \frac{\mathbf{I} : \mathbb{C} : \mathbf{I}}{\alpha^2} = \kappa$$

holds. This gives the final set of equations:

$$\int_\Omega \nabla^s \boldsymbol{\delta}_\mathbf{u} : \boldsymbol{\sigma} \left(\boldsymbol{\varepsilon} \right) - \int_\Omega \left(\mathbf{I} : \mathbb{T} : \nabla^s \boldsymbol{\delta}_\mathbf{u} \right) \hat{\kappa} \left(\hat{\varepsilon^v} - \mathbf{I} : \mathbb{T} : \nabla^s \mathbf{u} \right) = \int_\Omega \boldsymbol{\delta}_\mathbf{u} \cdot \mathbf{f} \qquad (46a)$$

$$- \int_\Omega \delta_{\hat{\varepsilon^v}} \hat{\kappa} \left(-\mathbf{I} : \mathbb{T} : \nabla^s \mathbf{u} + \hat{\varepsilon^v} \right) = 0 \quad (46b)$$

In essence, the mixed formulation we propose in the anisotropic case consists in taking as unknowns the displacement $\mathbf{u}$ and the modified volumetric strain

$$\hat{\varepsilon^v} = \mathbf{I} : \mathbb{T} : \nabla^s \mathbf{u} = \mathrm{Tr}(\mathbb{T} : \nabla^s \mathbf{u})$$

instead of $\varepsilon^v = \mathrm{Tr}(\nabla^s \mathbf{u}) = \nabla \cdot \mathbf{u}$.

3.3. Variational Multi-Scales stabilization

The discussion needs to be completed by the definition of a suitable stabilization. Proceeding similarly to the isotropic case, we can take a subgrid stabilization in the form (see Eqs. 17 with P_s the identity):

$$\mathbf{u}_s = \tau_1 \left[\mathbf{f} + \nabla \cdot \left(\mathbb{C} : \nabla^s \mathbf{u}_h + \hat{\kappa} \left(\hat{\varepsilon^v_h} - \mathbf{I} : \mathbb{T} : \nabla^s \mathbf{u}_h \right) \mathbf{I} \right) \right] \quad (47a)$$

$$\hat{\varepsilon^v_s} = \tau_2 \left(\mathbf{I} : \mathbb{T} : \nabla^s \mathbf{u}_h - \hat{\varepsilon^v_h} \right) \quad (47b)$$

Upon substitution in the Galerkin form we obtain, when using linear elements (see Eq. 20):

$$\int_\Omega \nabla^s \boldsymbol{\delta}_{\mathbf{u}_h} : \boldsymbol{\sigma} \left(\boldsymbol{\varepsilon}_h \right) + \int_\Omega \left(1 - \tau_2 \right) \left(\mathbf{I} : \mathbb{T} : \nabla^s \boldsymbol{\delta}_{\mathbf{u}_h} \right) \hat{\kappa} \left(\hat{\varepsilon^v_h} - \mathbf{I} : \mathbb{T} : \nabla^s \mathbf{u}_h \right)$$
$$= \int_\Omega \boldsymbol{\delta}_{\mathbf{u}_h} \cdot \mathbf{f} \quad (48a)$$

$$\int_\Omega \left(1 - \tau_2 \right) \delta_{\hat{\varepsilon^v_h}} \hat{\kappa} \left(\hat{\varepsilon^v_h} - \mathbf{I} : \mathbb{T} : \nabla^s \mathbf{u}_h \right)$$
$$+ \int_\Omega \tau_1 \hat{\kappa}^2 \nabla \delta_{\hat{\varepsilon^v_h}} \cdot \nabla \hat{\varepsilon^v_h} = - \int_\Omega \hat{\kappa} \nabla \delta_{\hat{\varepsilon^v_h}} \cdot \tau_1 \mathbf{f} \quad (48b)$$

3.4. Finite Element Implementation - Anisotropic case

As for the isotropic case the residual in FEM notation assumes a slightly different form depending on the choice of $\boldsymbol{\varepsilon}_h$. The option $\boldsymbol{\varepsilon}_h := \nabla^s \mathbf{u}_h - \frac{1}{\alpha} \nabla \cdot \mathbf{u}_h \, \mathbf{I} + \frac{1}{\alpha} \varepsilon^v_h \mathbf{I}$ gives

$$\mathbf{R}_I := \begin{pmatrix} N_I \mathbf{f}_{ext} - \mathbf{B}_I^t \boldsymbol{\sigma}(\boldsymbol{\varepsilon}_h) + \frac{1}{\alpha} \mathbf{B}_I^t \mathbf{C} \mathbf{T}^{-1} \mathbf{m} H_J - \left(1 - \tau_2 \right) \hat{\kappa} \boldsymbol{\Psi}_I^t H_J \\ \left(1 - \tau_2 \right) \hat{\kappa} N_I H_J + \hat{\kappa}^2 \mathbf{G}_I^t \tau_1 \mathbf{G}_J \varepsilon^v_{hJ} - \hat{\kappa} \mathbf{G}_I^t \tau_1 \mathbf{f} \end{pmatrix} \quad (49)$$

while the choice $\boldsymbol{\varepsilon}_h := \nabla^s \mathbf{u}_h$ results in

$$\mathbf{R}_I := \begin{pmatrix} N_I \mathbf{f}_{ext} - \mathbf{B}_I^t \boldsymbol{\sigma}(\boldsymbol{\varepsilon}_h) - \left(1 - \tau_2 \right) \hat{\kappa} \boldsymbol{\Psi}_I^t H_J \\ \left(1 - \tau_2 \right) \hat{\kappa} N_I H_J + \hat{\kappa}^2 \mathbf{G}_I^t \tau_1 \mathbf{G}_J \varepsilon^v_{hJ} - \hat{\kappa} \mathbf{G}_I^t \tau_1 \mathbf{f} \end{pmatrix} \quad (50)$$

with $\boldsymbol{\Psi}_J := \mathbf{m}^t \mathbf{T} \mathbf{B}_J$,

$$H_J := N_J \varepsilon^v_{hJ} - \boldsymbol{\Psi}^t_J \mathbf{u}_{hJ} \tag{51}$$

and

$$\hat{\kappa} := \frac{\mathbf{m}^t \mathbf{T}^{-t} \mathbf{C} \mathbf{T}^{-1} \mathbf{m}}{\alpha^2} \tag{52}$$

In either case, the LHS is identical and is given by

$$\mathbf{LHS}_{IJ} := \begin{pmatrix} \mathbf{B}^t_I \mathbf{C} \mathbf{B}_J - (1-\tau_2)\,\hat{\kappa} \boldsymbol{\Psi}_I \boldsymbol{\Psi}^t_J & (1-\tau_2)\,\hat{\kappa} \boldsymbol{\Psi}_I N_J \\ (1-\tau_2)\,\hat{\kappa} N_I \boldsymbol{\Psi}^t_J & -(1-\tau_2)\,\hat{\kappa} N_I N_J - \hat{\kappa}^2 \mathbf{G}^t_I \tau_1 \mathbf{G}_J \end{pmatrix} \tag{53}$$

4. Results

4.1. Manufactured solution test

We begin the result section by verifying the convergence rates of the proposed formulation. To that end, we employ the Method of Manufactured Solutions [19] and focus on a problem defined over a unit square, positioned so that the bottom left corner coincides with the position (0,0). The chosen target displacement field is

$$\bar{\mathbf{u}} = A \begin{pmatrix} \sin(4\pi x) \\ \cos(4\pi y) \\ 0 \end{pmatrix}$$

where A represents an adjustable amplification factor which in our tests is set to 10^{-3} to ensure that the solution remains well within the small strain regime. Such displacement field yields the volumetric strain field

$$\bar{\varepsilon^v} = 4\pi A \left(\cos(4\pi x) - \sin(4\pi y)\right)$$

The force field in equilibrium with such displacement can be obtained by substitution into Eq. 2 to give

$$\bar{\mathbf{f}} = (4\pi)^2 A \begin{pmatrix} C_{00} \sin(4\pi x) + C_{21} \cos(4\pi y) \\ C_{11} \cos(4\pi y) + C_{20} \sin(4\pi y) \\ 0 \end{pmatrix}$$

where the coefficients C_{ij} are the entries of the Voigt form of the constitutive tensor. For the sake of the benchmark, the domain is meshed using a linear quadrilateral structured mesh with 2^n lateral subdivisions. Different choices of the elastic parameters are employed with the aim of evaluating the performance in different conditions.

4.1.1. Incompressible isotropic material

A plain strain constitutive law with the material properties E and ν equal to 200 N/m^2 and 0.4999 is used with the aim of assessing the convergence at the incompressible limit.

Table 1 collects the $\mathbf{u}$ and ε^v error norms for each one of the meshes we use. These results are also depicted in Fig. 1. We observe that the convergence is quadratic for the $\mathbf{u}$ field and $h^{3/2}$ for the ε^v field.

Table 1: Incompressible isotropic material manufactured solution test. $\mathbf{u}$ and ε^v strain error norms.

n	1	2	3	4	5	6	7	8	9
h	0.5	0.25	0.125	6.25e-2	3.13e-2	1.56e-2	7.81e-3	3.91e-3	1.95e-3
$\|\mathbf{u}-\bar{\mathbf{u}}\|_{L^2(\Omega)}$	2.56e-1	3.57e-2	1.38e-2	2.60e-3	5.66e-4	1.34e-5	3.26e-5	8.06e-6	2.00e-6
$\|\varepsilon^v-\bar{\varepsilon^v}\|_{L^2(\Omega)}$	5.37e-2	1.95e-2	1.73e-3	5.37e-4	1.94e-4	6.56e-5	2.24e-5	7.79e-6	2.73e-6

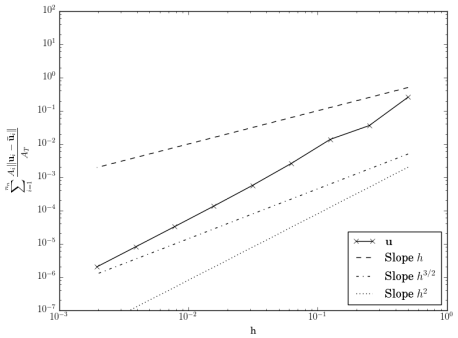

(a) $\mathbf{u}$ convergence.

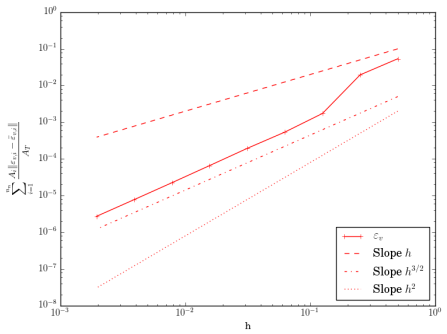

(b) ε^v convergence.

Figure 1: Manufactured solution test. Incompressible isotropic material convergence analysis. τ_1 computed with $\mathbb{C}$.

4.1.2. Anisotropic material

A plane-strain anisotropic material is checked next, using the constitutive tensor

$$\mathbb{C} = \begin{pmatrix} 54469.29 & 8284.82 & 17726.94 \\ 8284.82 & 5981.77 & 2615.99 \\ 17726.94 & 2615.99 & 8305.89 \end{pmatrix} \tag{54}$$

The calculated $\mathbf{C}_{iso}$ and $\mathbf{T}$ matrices are

$$\mathbf{C}_{iso} = \begin{pmatrix} 29692.637 & 8817.713 & 0. \\ 8817.713 & 29692.637 & 0. \\ 0. & 0. & 10437.462 \end{pmatrix} \tag{55}$$

and

$$\mathbf{T} = \begin{pmatrix} 1.32161932 & 0.0931325 & 0.35389397 \\ -0.04531568 & 0.41023417 & -0.01086188 \\ 0.58737628 & 0.07153362 & 0.66756935 \end{pmatrix} \tag{56}$$

We recall that in the anisotropic case the obtained "volumetric strain" is not any longer $\nabla \cdot \mathbf{u}$ but instead $\mathbf{I} : \mathbb{T} : \nabla^s \mathbf{u}_h$. After computing the anisotropy matrix $\mathbb{T}$ corresponding to the constitutive matrix in Eq. 54 we obtain the analytical volumetric strain field $\bar{\varepsilon^v} = 4\pi A \left(1.2763 \cos\left(4\pi x\right) - 0.503367 \sin\left(4\pi y\right)\right)$.

Table 2 collects the $\mathbf{u}$ and $\hat{\varepsilon^v}$ error norms for each one of the meshes we use. These results are also depicted in Fig. 2.

Table 2: Anisotropic material manufactured solution test. $\mathbf{u}$ and ε^v strain error norms.

n	1	2	3	4	5	6	7	8	9
h	0.5	0.25	0.125	6.25e-2	3.13e-2	1.56e-2	7.81e-3	3.91e-3	1.95e-3
$\|\mathbf{u} - \bar{\mathbf{u}}\|_{L^2(\Omega)}$	2.08e-2	1.94e-3	2.58e-3	1.33e-3	4.11e-4	1.09e-4	2.76e-5	6.92e-6	1.73e-6
$\|\hat{\varepsilon^v} - \bar{\varepsilon^v}\|_{L^2(\Omega)}$	1.94e-2	1.61e-2	2.13e-2	9.89e-3	3.03e-3	8.05e-4	2.07e-4	5.36e-5	1.41e-5

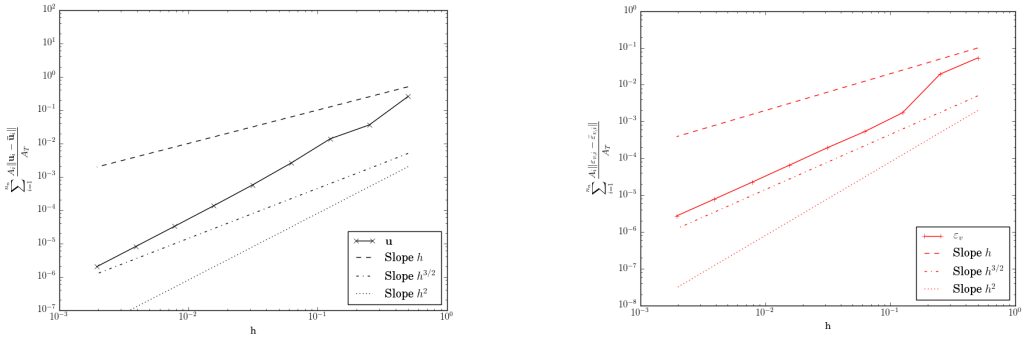

(a) $\mathbf{u}$ convergence.

(b) **mTBu** convergence.

Figure 2: Manufactured solution test. Anisotropic material convergence analysis. τ_1 computed with $\mathbb{C}$.

4.2. Cook's membrane

The second benchmark test considered is the well known Cook's membrane benchmark, described for example in [5]. The setup of the test is shown

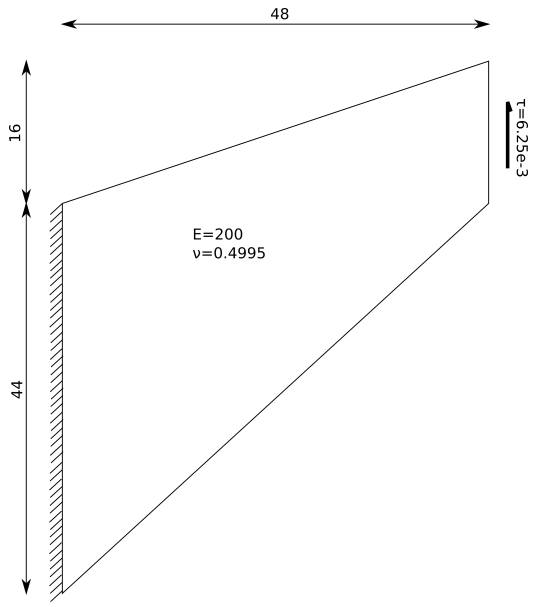

Figure 3: Setup of Cook's Membrane Benchmark [mm].

in Fig. 3. The test is run employing the proposed formulation using both triangles (irreducible and mixed) and quads (irreducible, mixed and Bbar). The test is also run in plane strain and in 3D.

4.2.1. Incompressible isotropic material

We firstly conduct the test using a linear elastic plane strain constitutive law with the material properties stated in Fig. 3. The plot of the y-displacement on the top right point is shown in Fig. 4 for a uniform mesh subdivisions by factors 2-2^9. We observe that the proposed formulation converges much faster to the expected value than the irreducible one. When comparing to the Q1P0 (Bbar) element, this shows a slightly better behaviour for the coarser meshes.

Complementarily, we solve the problem for a set of unstructured triangular meshes whose sizes can be computed as $5/2^n$, $n \in (0, 6)$. Fig. 5 depicts the y-displacement convergence on the top right point. The superior performance of the mixed $\mathbf{u}$-ε^v formulation becomes evident in this case.

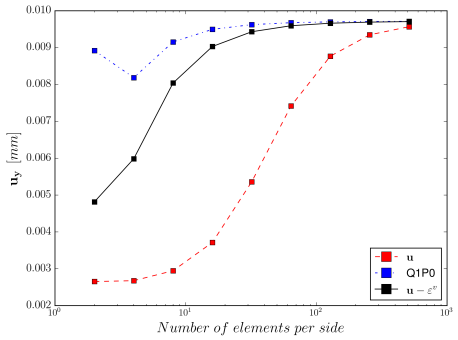

(a) Quadrilateral elements.

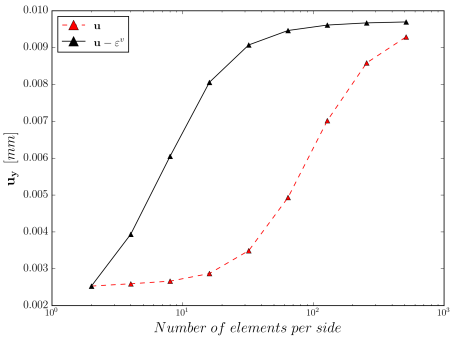

(b) Triangular elements.

Figure 4: Cook's membrane test. Incompressible isotropic material u_y structured meshes convergence results.

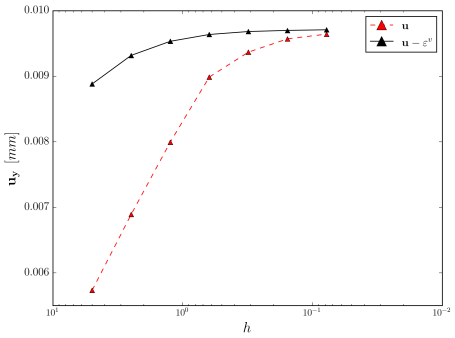

Figure 5: Cook's membrane test. Incompressible isotropic material u_y unstructured triangular mesh convergence results.

Finally, we also present a view of selected results in Fig. 6 showing that a good solution is found in all the variables of interest.

4.2.2. Incompressible anisotropic material

We carry out the same test but using an incompressible anisotropic material whose response is modelled by the constitutive tensor

$$\mathbb{C} = \begin{pmatrix} 970870.07 & 1239555.39 & 0.0 \\ 1239555.39 & 1622077.42 & 0.0 \\ 0.0 & 0.0 & 6711.41 \end{pmatrix}$$

with the associate $\mathbf{C}_{iso}$ and $\mathbf{T}$ matrices

$$\mathbf{C}_{iso} = \begin{pmatrix} 1292124.1915 & 1243904.9435 & 0. \\ 1243904.9435 & 1292124.1915 & 0. \\ 0. & 0. & 24109.624 \end{pmatrix} \tag{57}$$

and

$$\mathbf{T} = \begin{pmatrix} 0.34121548 & -0.20655167 & 0. \\ 0.53340404 & 1.31787552 & 0. \\ 0. & 0. & 0.52760836 \end{pmatrix} \tag{58}$$

Fig. 7 presents the convergence results. Once again, the proposed mixed formulation far outperforms the irreducible approach.

4.3. Bimaterial Cook's membrane

4.3.1. Two isotropic materials

As a third test, we modify the second benchmark by introducing two different materials as shown in Fig. 8. Only one of the two materials is considered incompressible in order to introduce a large difference in the constitutive behaviour. Thus, the E and ν are 2.0×10^4 Pa and 0.4995 in the top half of the membrane while they are 2.0×10^2 and 0.3 in the bottom one.

We shall remark that introducing a discontinuity in the material is classically challenging for mixed approaches, but the proposed approach seems to handle the case without difficulties, thus proving that one of the design goals of the method is accomplished.

The plot of vertical displacement vs mesh subdivision for such configuration is shown in Fig. 9.

Fig. 10 shows a view of the $\mathbf{u}$, ε^v and stress fields showing that no spurious oscillations are found.

4.3.2. Isotropic - anisotropic materials

We repeat the same bimaterial Cook's membrane example but substituting the isotropic material in the bottom half of the membrane by the anisotropic one characterized by the constitutive tensor

$$\mathbb{C} = \begin{pmatrix} 54469.29 & 8284.82 & 17726.94 \\ 8284.82 & 5981.77 & 2615.99 \\ 17726.94 & 2615.99 & 8305.89 \end{pmatrix}$$

The plot of vertical displacement vs mesh subdivision for such configuration is shown in Fig. 11.

Fig. 12 shows a view of the $\mathbf{u}$, ε^v and stress fields showing that no spurious oscillations are found.

4.4. 3D anisotropic Cook's membrane

We extrude the same geometry 16 mm. The surface load is now 1.0×10^5 N/mm^2. We fix the out of plane displacements in the front and rear surfaces. The anisotropic constitutive tensor we use is

$$\mathbf{C}_{aniso} := \begin{pmatrix} 5.99E+11 & 5.57E+11 & 5.34E+11 & 0 & 0 & 4.44E+09 \\ 5.57E+11 & 5.71E+11 & 5.34E+11 & 0 & 0 & -3.00E+09 \\ 5.34E+11 & 5.34E+11 & 5.37E+11 & 0 & 0 & 9.90E+05 \\ 0 & 0 & 0 & 1.92E+09 & 9.78E+06 & 0 \\ 0 & 0 & 0 & 9.78E+06 & 2.12E+09 & 0 \\ 4.44E+09 & -3.00E+09 & 9.90E+05 & 0 & 0 & 2.56E+10 \end{pmatrix} \quad (59)$$

We use an unstructured mesh conformed by around 230k linear tetrahedral elements (Fig 13).

As can be seen in Fig. 14 smooth results are obtained for all the fields thus confirming that the formulation also works correctly in the 3D case.

4.5. 3D necking bar

The objective of the benchmark is to compare the behaviour of the proposed formulation, using both a structured and unstructured discretization, to a reference Bbar implementation in a case involving plasticity. To that purpose we solve the well-known necking bar example using a perfect isotropic J2 plasticity law. The Young modulus, Poisson ratio, and yield stress are 210×10^9 GPa, 0.29 and 200 MPa respectively. The specimen, whose dimensions are $5.4 \times 0.5 \times 0.2$ cm^3, is clamped in its left face while an incremental total displacement of 0.006 cm is imposed in its right face.

A structured hexahedral mesh conformed by 4.4k elements (Fig. 15) is employed. A fairly similar discretization level in terms of element sizes is achieved with an unstructured mesh of around 33k tetrahedras (Fig. 16).

Figs. 17 and 18 present the plastic dissipation and the uniaxial stress obtained for the three cases. As it can be observed in Fig. 18 the final deformed shape and the uniaxial stress distribution is very similar in all the cases. No spurious oscillations are visible in the mixed solution. Plastic dissipation is slightly underestimated in the unstructured mesh results, probably because of a slightly stiffer behaviour of the tetrahedral element.

4.6. Automotive machinery piece

This last example presents the (purely qualitative) results of a simulation involving the plastic deformation of an industrial piece. The problem consists in the mechanical analysis of an aluminium object from the automotive industry. The specimen (Fig. 19) has a length around 280 mm and a thickness of 8.5 mm. It is clamped in the magenta region in Fig. 19c. A surface load of 300 kPa is incrementally applied in the yellow region in Fig. 19c.

The material response is modeled using an isotropic small strain perfect J2 plasticity law. E and ν are set to 70 GPa and 0.35. The plastic regime is characterized by the yield stress $\sigma_y = 120$ MPa. Such material model implies a quasi-incompressible behaviour within the plastic region (implying that the volumetric deformation will be small compared to the total deformation), thus making unappealing the use of low order irreducible elements. The complexity of the shape prevents the use of B-bar type hexahedral meshes, thus leaving the proposed $\mathbf{u}$-ε^v technology as one of the few possible alternatives.

The domain was meshed using 550k linear tetrahedra, employing the proposed mixed formulation.

Figs. 20 and 21 depict the obtained results. The piece shows a rather ductile behaviour up to the point at which a plastic hinge appears in the vicinity of the clamping (Fig. 21c).

Fig. 21 collects a set of snapshots describing the evolution of the plastic deformation. More specifically, it can be noted that prior to the formation of the plastic hinge at the basis, large parts of the specimen reach the yield stress (120 MPa) (Figs. 21a and 21b) and thus present a plastic energy dissipation (Fig. 21c).

5. Conclusion

The paper presents a novel mixed element, able to tackle the quasi-incompressible limit. The proposed formulation aims at addressing problems with material nonlinearity, and is effective also in presence of multiple material interfaces. A convenient modification, that allows dealing with initially anisotropic problems is described. The proposed mixed method is proved effective in combination with a plastic material behaviour.

Acknowledgements

This research has been partly supported by the European Commission (EC) through the project ExaQUte (H2020-FETHPC-2016-2017-800898).

The authors also acknowledge financial support from the Spanish Ministry of Economy and Competitiveness , through the "Severo Ochoa Programme for Centres of Excellence in R& D" (CEX2018-000797-S). R. Zorrilla gratefully acknowledges the support of the Spanish ministry of Science, Innovation and Universities for his FPU grant (FPU15/03796). R. Codina acknowledges the support received from the ICREA Acadèmia Research Program, from the Catalan Government.

References

[1] M. Chiumenti, Q. Valverde, C. A. de Saracibar, M. Cervera, A stabilized formulation for incompressible elasticity using linear displacement and pressure interpolations, Computer Methods in Applied Mechanics and Engineering 191 (2002) 5253 – 5264. doi:10.1016/S0045-7825(02)00443-7.

[2] M. de Mier Torrecilla, Numerical simulation of multi-fluid flows with the Particle Finite Element Method, Ph.D. thesis, Universitat Politècnica de Catalunya. Departament de Resistència de Materials i Estructures a l'Enginyeria, 2010.

[3] N. Abboud, G. Scovazzi, Elastoplasticity with linear tetrahedral elements: A variational multiscale method, International Journal for Numerical Methods in Engineering 115 (2018) 913–955. doi:10.1002/nme.5831.

[4] M. Cervera, M. Chiumenti, R. Codina, Mixed stabilized finite element methods in nonlinear solid mechanics: Part i: Formulation, Computer Methods in Applied Mechanics and Engineering 199 (2010) 2559 – 2570. doi:10.1016/j.cma.2010.04.006.

[5] M. Chiumenti, M. Cervera, R. Codina, A mixed three-field fe formulation for stress accurate analysis including the incompressible limit, Computer Methods in Applied Mechanics and Engineering 283 (2015) 1095 – 1116. doi:10.1016/j.cma.2014.08.004.

[6] P. Dadvand, R. Rossi, E. Oñate, An object-oriented environment for developing finite element codes for multi-disciplinary applications, Archives of Computational Methods in Engineering 17 (2010) 253–297. doi:10.1007/s11831-010-9045-2.

[7] P. Dadvand, R. Rossi, M. Gil, X. Martorell, J. Cotela, E. Juanpere, S. Idelsohn, E. Oñate, Migration of a generic multi-physics framework to hpc environments, Computers & Fluids 80 (2013) 301 – 309. doi:10.1016/j.compfluid.2012.02.004.

[8] N. Lafontaine, R. Rossi, M. e. a. Cervera, Explicit mixed strain-displacement finite element for dynamic geometrically non-linear solid mechanics, Computational Mechanics 55 (2015) 543–559. doi:10.1007/s00466-015-1121-x.

[9] M. Cervera, N. Lafontaine, R. e. a. Rossi, Explicit mixed strain–displacement finite elements for compressible and quasi-incompressible elasticity and plasticity, Computational Mechanics 58 (2016) 511–532. doi:10.1007/s00466-016-1305-z.

[10] M. Destrade, P. Martin, T. Ting, The incompressible limit in linear anisotropic elasticity, with applications to surface waves and elastostatics, Journal of the Mechanics and Physics of Solids 50 (2002) 1453–1468. doi:https://doi.org/10.1016/S0022-5096(01)00121-1.

[11] S. Federico, A. Grillo, S. Imatani, The linear elasticity tensor of incompressible materials, Mathematics and Mechanics of Solids 20 (2015). doi:https://doi.org/10.1177/1081286514550576.

[12] T. J. Hughes, G. R. Feijóo, L. Mazzei, J.-B. Quincy, The variational multiscale method—a paradigm for computational mechanics, Computer Methods in Applied Mechanics and Engineering 166 (1998) 3 – 24. doi:10.1016/S0045-7825(98)00079-6, advances in Stabilized Methods in Computational Mechanics.

[13] R. Codina, S. Badia, J. Baiges, J. Principe, *Variational Multiscale Methods in Computational Fluid Dynamics*, in Encyclopedia of Computational Mechanics (eds E. Stein, R. Borst and T.J.R. Hughes), John Wiley & Sons Ltd., 2017, pp. 1–28. doi:10.1002/9781119176817.ecm2117.

[14] R. Codina, J. Principe, J. Baiges, Subscales on the element boundaries in the variational two-scale finite element method, Computer Methods in Applied Mechanics and Engineering 198 (2009) 838–852.

[15] R. Codina, Stabilization of incompressibility and convection through orthogonal sub-scales in finite element methods, Computer Methods in Applied Mechanics and Engineering 190 (2000) 1579–1599.

[16] R. Codina, Analysis of a stabilized finite element approximation of the Oseen equations using orthogonal subscales, Applied Numerical Mathematics 58 (2008) 264–283.

[17] J. Baiges, R. Codina, Variational Multiscale error estimators for solid mechanics adaptive simulations: An Orthogonal Subgrid Scale approach, Computer Methods in Applied Mechanics and Engineering 325 (2017) 37–55. doi:10.1016/j.cma.2017.07.008.

[18] A. Norris, The isotropic material closest to a given anisotropic material, Journal of Mechanics of Materials and Structures 1 (2005). doi:10.2140/jomms.2006.1.223.

[19] P. J. Roache, Code Verification by the Method of Manufactured Solutions , Journal of Fluids Engineering 124 (2001) 4–10. doi:10.1115/1.1436090.

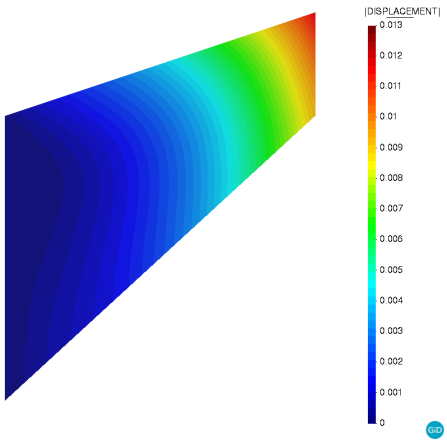

(a) $\|\mathbf{u}\|$

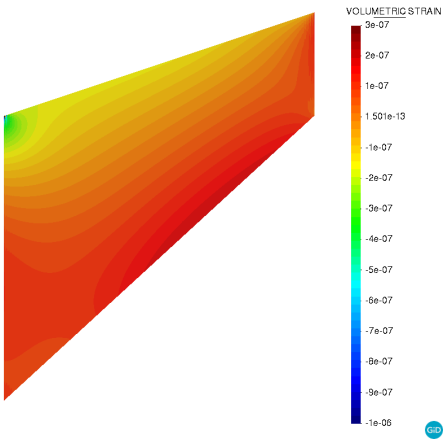

(b) ε^v

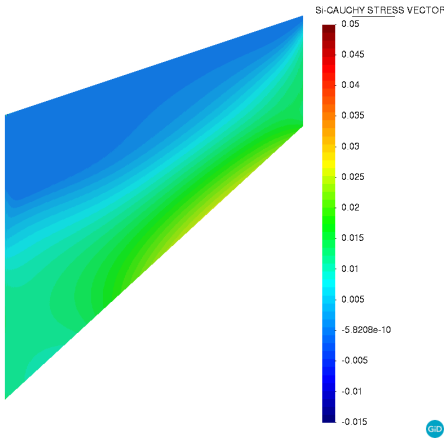

(c) S_1

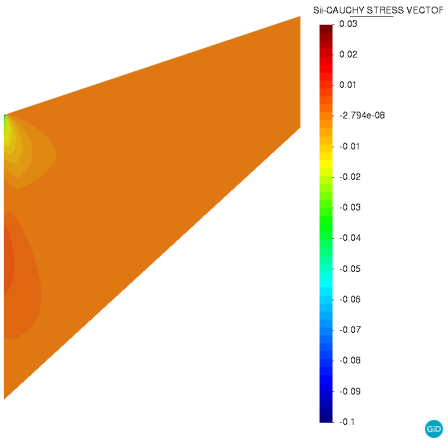

(d) S_2

Figure 6: Cook's membrane test. Solution snapshots for the 256 divisions quadrilateral mesh (S_1, S_2: principal stresses).

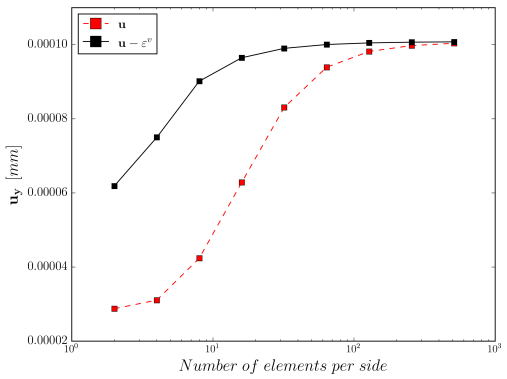

Figure 7: Cook's membrane test. Incompressible anisotropic material u_y convergence results.

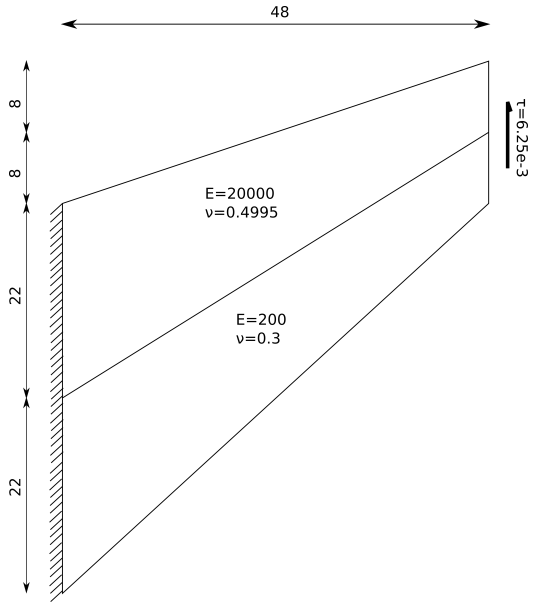

Figure 8: Setup of Cook's Membrane Benchmark using two distinct materials.

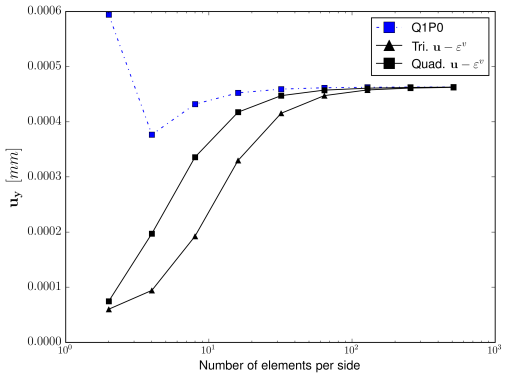

Figure 9: Bimaterial Cook's membrane test. u_y convergence.

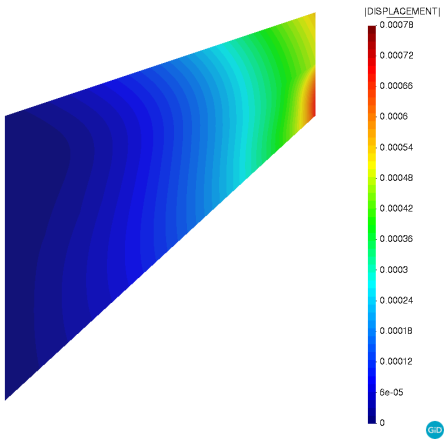

(a) $\|\mathbf{u}\|$

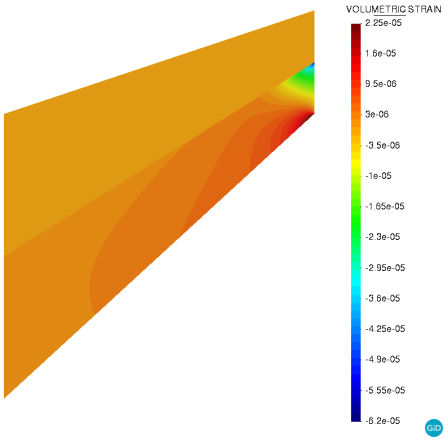

(b) ε^v

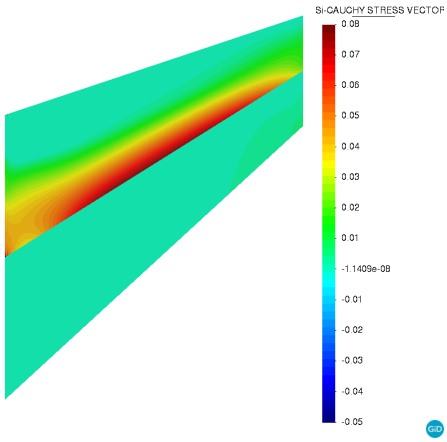

(c) S_1

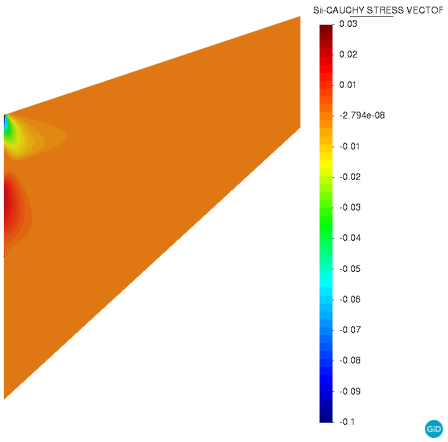

(d) S_2

Figure 10: Bimaterial Cook's membrane test. Solution snapshots for the 256 divisions quadrilateral mesh.

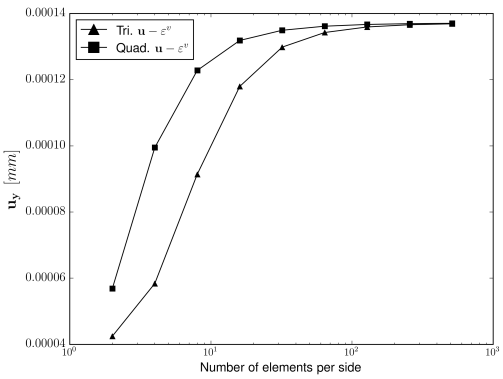

Figure 11: Bimaterial (isotropic - anisotropic) Cook's membrane test. u_y convergence.

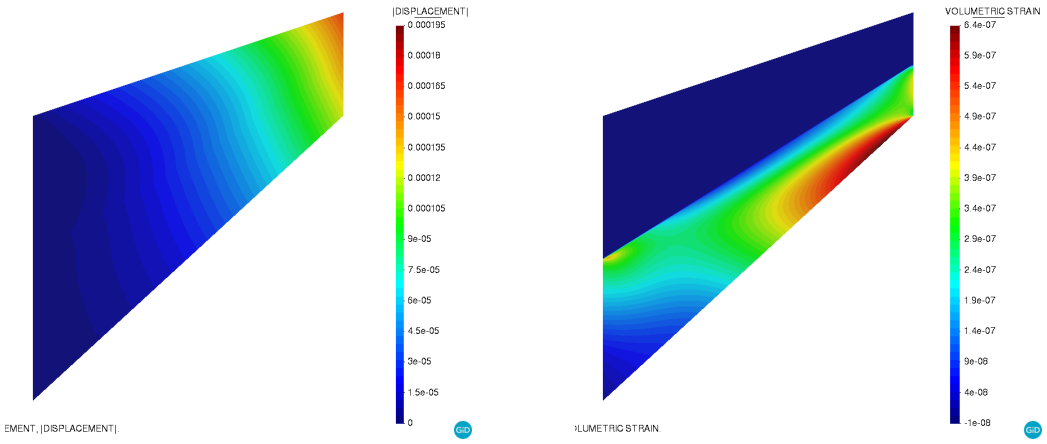

(a) $\|\mathbf{u}\|$ (b) ε^v

(c) S_1 (d) S_2

Figure 12: Bimaterial (isotropic - anisotropic) Cook's membrane test. Solution snapshots for the 256 divisions quadrilateral mesh.

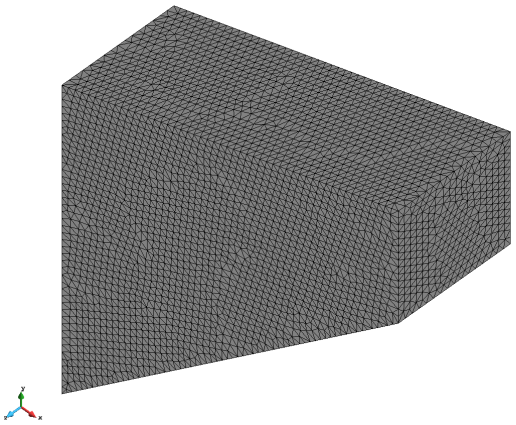

Figure 13: 3D anisotropic Cook's membrane. Unstructured linear tetrahedra mesh.

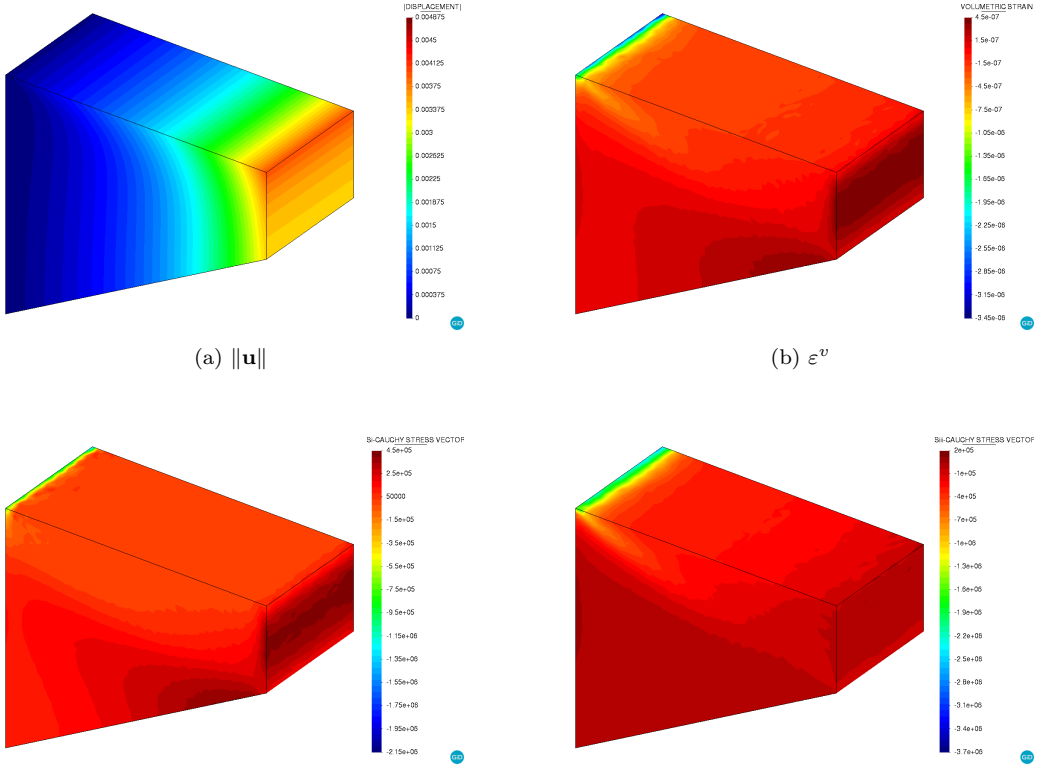

(a) $\|\mathbf{u}\|$ (b) ε^v

(c) S_1 (d) S_3

Figure 14: 3D anisotropic Cook's membrane. Solution snapshots.

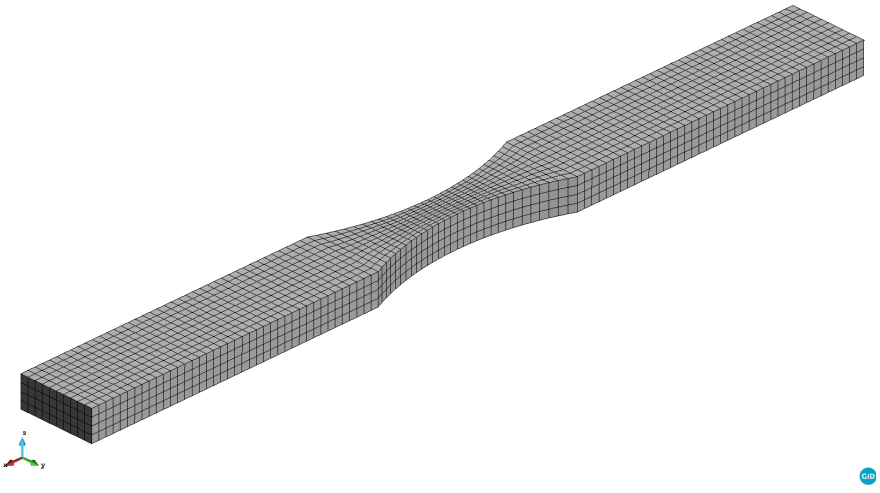

(a) Isometric view.

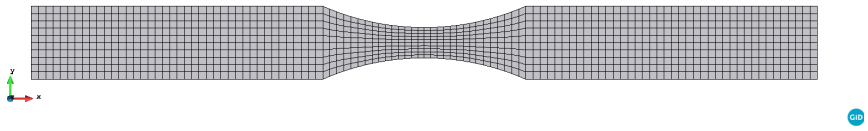

(b) xy-plane view.

Figure 15: 3D necking bar. Structured hexaedra mesh.

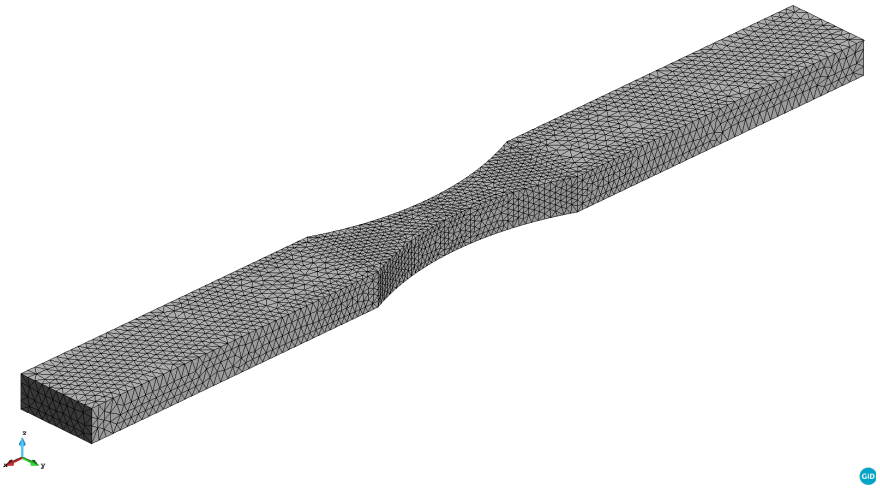

(a) Isometric view.

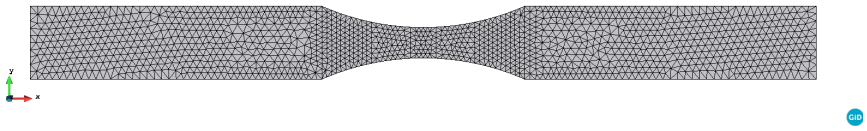

(b) xy-plane view.

Figure 16: 3D necking bar. Structured tetrahedra mesh.

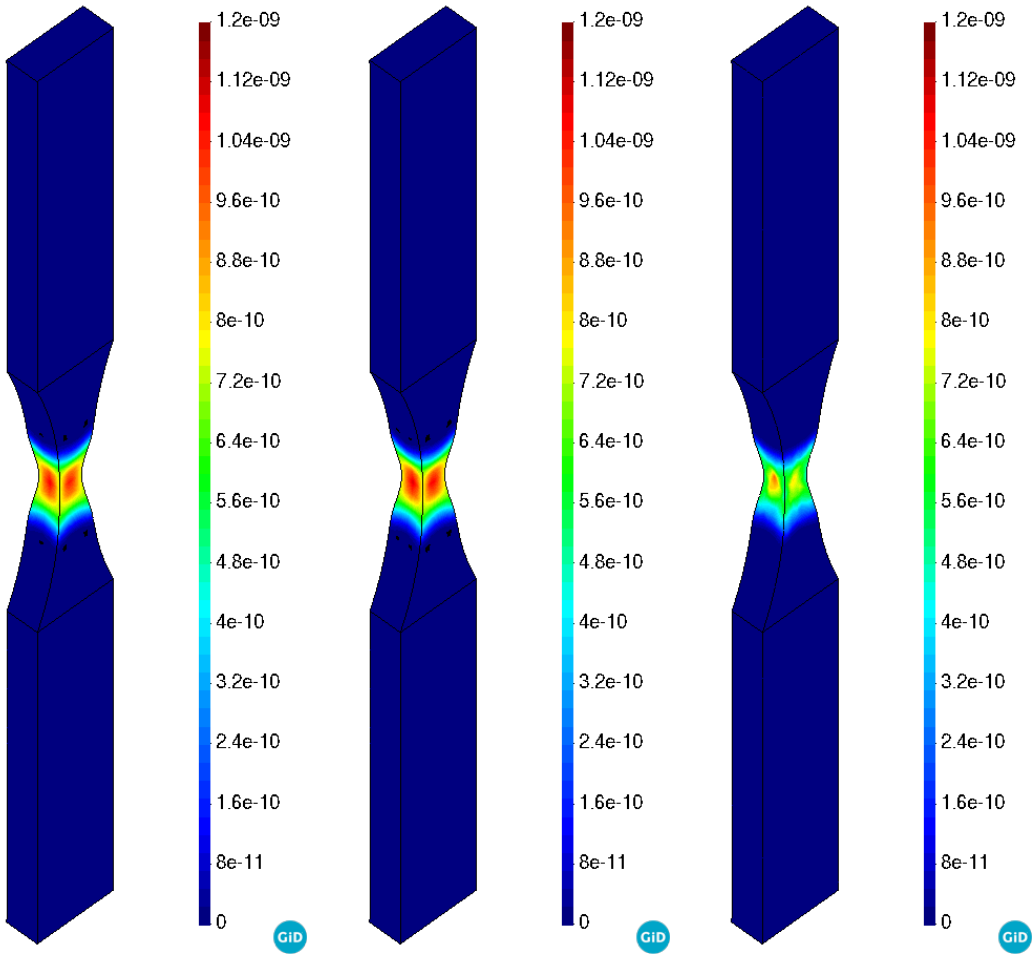

(a) Bbar. (b) $\mathbf{u}$-ε^v hexaedra. (c) $\mathbf{u}$-ε^v tetrahedron.

Figure 17: 3D necking bar. Plastic dissipation (deformation scale x40).

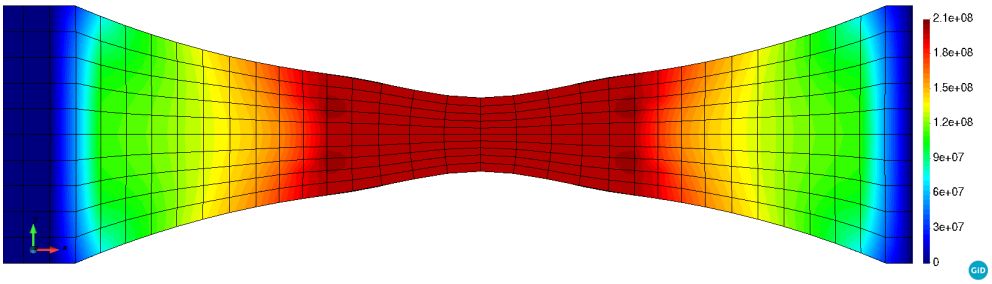

(a) Bbar.

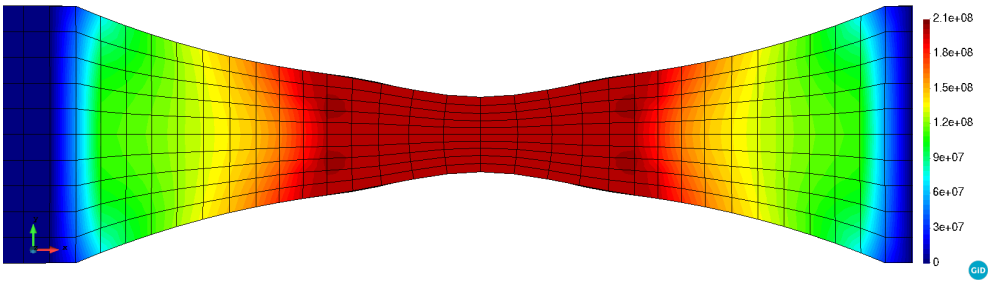

(b) $\mathbf{u}$-ε^v hexaedra.

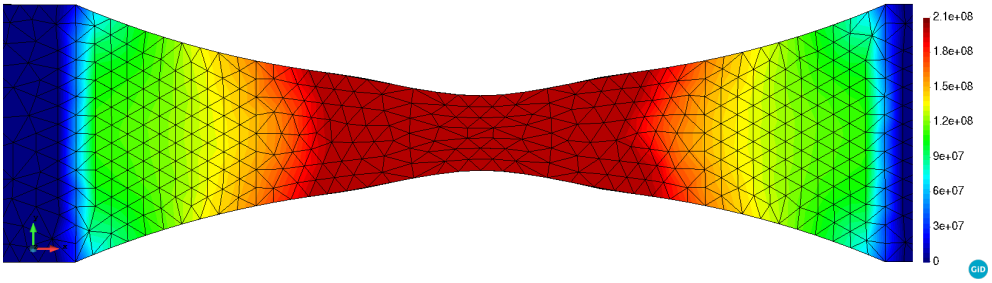

(c) $\mathbf{u}$-ε^v tetrahedron.

Figure 18: 3D necking bar. Uniaxial stress [Pa] (deformation scale x40).

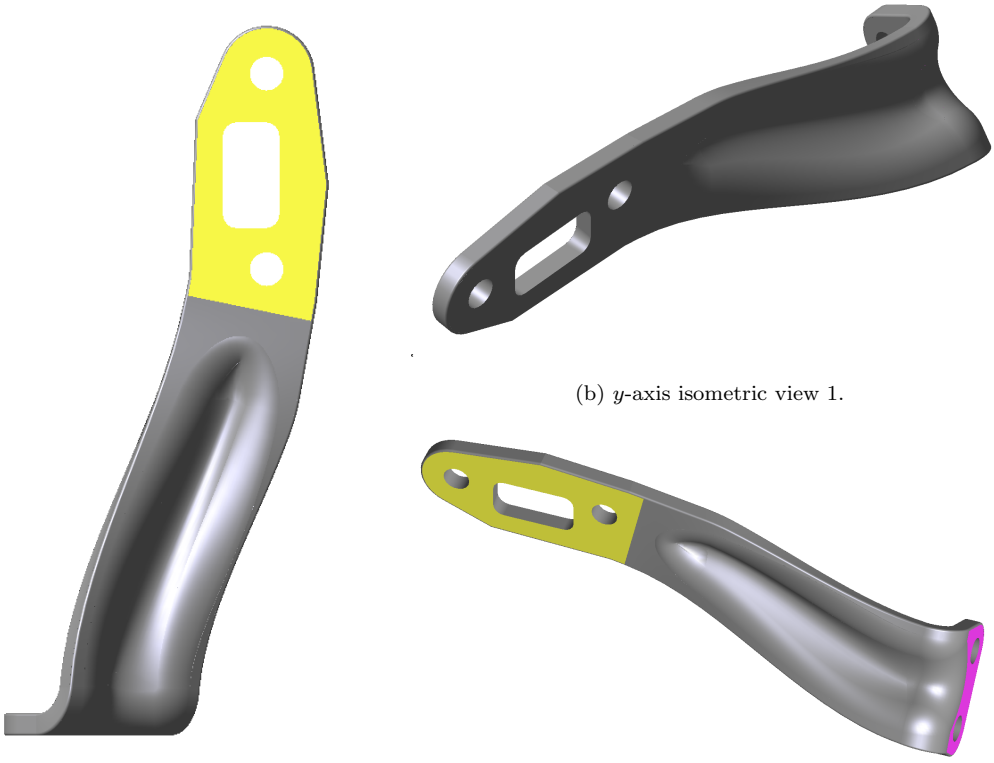

(a) yz-plane view.

(b) y-axis isometric view 1.

(c) y-axis isometric view 2.

Figure 19: Automotive machinery piece. Problem geometry.

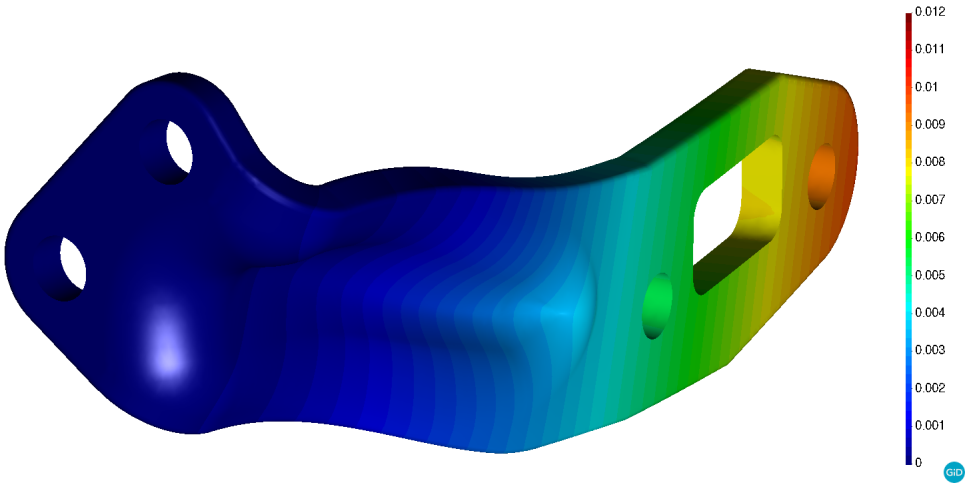

Figure 20: Automotive machinery piece. $\|\mathbf{u}\|$ [m].

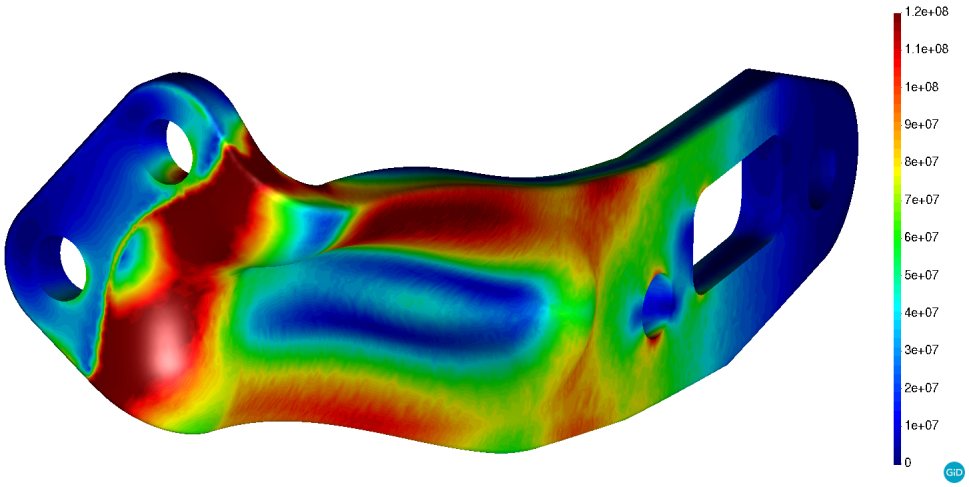

(a) Uniaxial stress rear view [Pa] (deformation scale ×5).

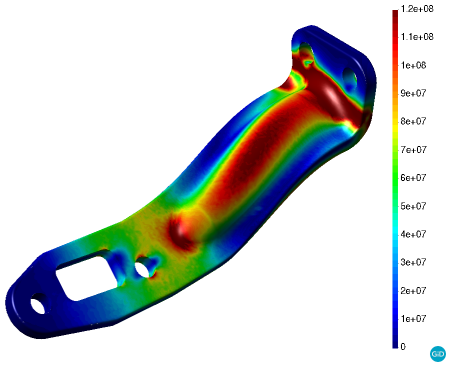

(b) Uniaxial stress lateral view [Pa].

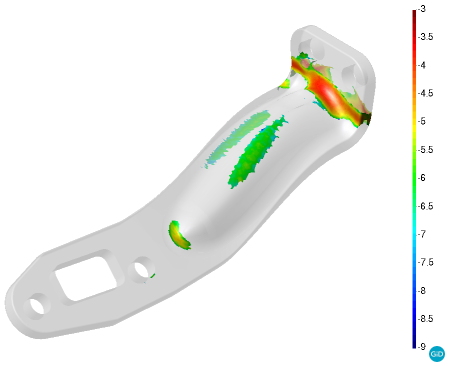

(c) Plastic dissipation (log scale).

Figure 21: Automotive machinery piece. Plasticity magnitudes isometric view.